Platelet C3G protects from liver fibrosis, while enhancing tumor growth through regulation of the immune response

Cristina Baquero[1,2], Minerva Iniesta-González[1,2]*, Nerea Palao[1,2]*, Cristina Fernández-Infante[3,4], Mateo Cueto-Remacha[1,2], Jaime Mancebo[1,2], Samuel de la Cámara-Fuentes[5], María Rodrigo-Faus[1,2], M. Pilar Valdecantos[6,7], Angela M Valverde[6,7], Celia Sequera[1,8], Sara Manzano[1], Ángel M. Cuesta[1,2], Alvaro Gutierrez-Uzquiza[1,2], Paloma Bragado[1,2+], Carmen Guerrero[3,4,9§+], Almudena Porras[1,2§+]

[1]Departamento de Bioquímica y Biología Molecular, Facultad de Farmacia, Universidad Complutense de Madrid, 28040 Madrid, Spain.
[2]Instituto de Investigación Sanitaria del Hospital Clínico San Carlos (IdISSC), 28040 Madrid, Spain.
[3]Instituto de Biología Molecular y Celular del Cáncer (IMBCC), Universidad de Salamanca-CSIC, 37007 Salamanca, Spain.
[4]Instituto de Investigación Biomédica de Salamanca (IBSAL), 37007 Salamanca, Spain.
[5]Unidad de Proteómica, Centro de Técnicas Biológicas, Universidad Complutense de Madrid, 28040 Madrid, Spain.
[6]Instituto de Investigaciones Biomédicas (IIBM) Alberto Sols-Morreale (CSIC-UAM), 28029 Madrid, Spain.
[7]Centro de Investigación Biomédica en Red de Diabetes y Enfermedades Metabólicas Asociadas (CIBERdem), Instituto de Salud Carlos III, Madrid, Spain.
[8]Aix Marseille Univ, CNRS, Inserm, Institut Paoli-Calmettes, Centre de Recherche en Cancérologie de Marseille (CRCM), Marseille, France
[9]Departamento de Medicina, Universidad de Salamanca, 37007 Salamanca, Spain.

*Equally contributed to this work
[§]Correspondence: A. Porras, Departamento de Bioquímica y Biología Molecular, Facultad de Farmacia, UCM, Ciudad Universitaria, Madrid, Spain. Tel.: +34 913941627; e-mail: maporras@ucm.es. Co-correspondence: C. Guerrero, Centro de Investigación del Cáncer, Campus Unamuno s/n, Salamanca, Spain. Tel.: +34 923294801; fax.: +34 923294795; e-mail: cguerrero@usal.es.
[+]Co-seniors investigators

Running title: Platelet C3G reduces fibrosis, while favoring liver cancer growth

Keywords: C3G (RapGEF1), platelets, liver fibrosis, liver cancer, immune response

Abbreviations: CLD (chronic liver disease); HCC (hepatocellular carcinoma); CCL2/5 ((C-C motif) ligand 2/5); CXCL8/10 ((C-X-C motif) ligand 8/10), HGF (hepatocyte growth factor), TGF-β (transforming growth factor-β), CXCL4/7((C-X-C motif) ligand 4/7)); PF4 (platelet factor 4); IL-6 (Interleukin-6); ALT (alanine aminotransferase); AST (aspartate amino transferase); MASH (metabolic dysfunction–associated steatohepatitis); NASH (non-alcoholic steatohepatitis); NAFLD (non-alcoholic liver disease); MAFLD (metabolic dysfunction–associated liver disease); Glycoprotein V (GPV); BMP1 (Bone morphogenetic protein 1); Arg1 (Arginase 1); Thrombospondin 1 (Thbs1); Syntaxin 11 (Stx11); Ngp (Neutrophil granule protein); Saa2 (Serum amyloid A2); SOD1 (Superoxide-dismutase1); Slamf1 (Signaling lymphocytic activation molecule family member 1); VASP (Vasodilator-Stimulated Phosphoprotein); Snap23 (Synaptosome Associated Protein 23); GP1bb (Platelet Glycoprotein Ib Beta Chain).

Abstract

Primary liver cancer usually occurs in the context of chronic liver disease (CLD), being associated with fibrosis. Platelets have emerged as important regulators of CLD and liver cancer, although their precise function and mechanism of action need to be clarified. C3G (RapGEF1) regulates platelet activation, adhesion and secretion. Here, we have evaluated the role of platelet C3G in chemically-induced fibrosis and liver cancer associated with fibrosis using genetically modified mouse models. We found that while overexpression of full-length C3G in platelets decreased liver fibrosis induced by chronic treatment with CCl_4, overexpressed C3G lacking the catalytic domain did not, although in both cases platelet recruitment to the liver was similar. In addition, C3G deletion in platelets (PF4-C3GKO mouse model) increased CCl_4-induced liver damage and hepatic fibrosis, reducing liver platelets and macrophages. Moreover, early liver immune response to CCl_4 was altered in PF4-C3GKO mice, being remarkable the lower activation of macrophages and the increased monocyte-derived macrophages compared to wt mice. On the other hand, in response to DEN+CCl_4, PF4-C3Gwt mice exhibited more, and larger liver tumors than PF4-C3GKO mice, accompanied by the presence of more platelets, despite having less fibrosis in previous steps. Liver immune cell populations were also differentially regulated in PF4-C3GKO mice, highlighting the higher number of macrophages, likely with a pro-inflammatory phenotype, present in the liver in response to chronic DEN+CCl_4 treatment. Proteins upregulated or downregulated in platelet-rich plasma from PF4-C3GKO compared to wt mice might regulate the immune response and tumor development. In this regard, enrichment analyses using proteomic data showed changes in several proteins involved in platelet activation and immune response pathways. Additionally, the higher secretion of CD40L by PF4-C3GKO platelets could contribute to their anti-tumor effect. Therefore, platelet C3G presents anti-fibrotic and pro-tumoral effects in the liver, likely mediated by changes in the immune response.

Introduction

Chronic liver disease (CLD), a major global health problem, can lead to liver cancer, the sixth most common cancer [1, 2]. Fibrosis, a hallmark of CLD, can progress to cirrhosis, the main risk factor for the development of hepatocellular carcinoma (HCC), the most frequent liver cancer [2]. However, the causal relationship between fibrosis and HCC development remains unclear [3].

Hepatic injury activates fibrogenesis, which involves extracellular matrix (ECM) secretion [4, 5] and induces regeneration, which requires hepatocyte proliferation. However, when liver damage becomes chronic, hepatocyte proliferation is impaired, and hepatic progenitor/oval cells are activated and expanded as an alternative regeneration mechanism [4, 6].

Liver fibrosis and HCC development are complex processes regulated by several signals such as growth factors (e.g. TGF-β), cytokines (e.g. IL-6) and chemokines (e.g. CCL2/5), arising from the interaction of different liver cell types, mainly hepatic stellate cells (HSCs), hepatocytes, Kupffer cells (KCs) (resident macrophages) and infiltrated immune cells [2, 5, 7, 8]. HSCs and cancer-associated fibroblasts are the main ECM producers [3]. During chronic injury HSCs become activated, transdifferentiate into myofibroblasts, express α-smooth muscle actin (α-SMA) and secrete ECM, mainly collagen type I and III, promoting fibrosis and chronic inflammation [4, 9–11]. All this can

contribute to maintaining hepatic fibrogenesis and/or to liver repair depending on the context.

In HCC, immune cells play a dual role depending on the context and timing [2]. A better prognosis is associated with the existence of immune infiltrates in HCC patients owing to the capacity of $CD8^+$ cytotoxic T cells to kill cancer cells [12]. However, in metabolic dysfunction–associated steatohepatitis (MASH) (formerly non-alcoholic steatohepatitis (NASH)) mouse models, $CD8^+$T cells showed a pro-inflammatory and pro-tumorigenic role, facilitated by platelet-mediated recruitment [13].

Platelets are key players in fibrosis, CLD and HCC. Under physiological conditions, platelets maintain liver homeostasis, vascular integrity, and regulate the immune system [14, 15]. In CLD their function seems to be dual. Higher platelet levels correlate with less fibrosis in CLD patients [15] owing to the increased release of anti-fibrotic factors (e.g. HGF) and the decrease in TGF-β [16]. However, platelets also exacerbate local inflammation by recruiting different immune cells [13] and secrete pro-fibrotic factors such as TGF-β, PDGF and CXCL4 (also named PF4) [14].

In HCC, as in other cancers [17], platelets can also have a dual function. On one side, thrombocytosis has been associated with worse overall survival [18, 19] and thrombocytopenia with better outcomes of HCC patients [20]. As HCC promoters, platelets can induce hepatocyte proliferation [14], angiogenesis, and monocyte recruitment. Platelet releasates also facilitate a switch from monocytes to pro-tumoral macrophages, favoring HCC progression [15]. Platelets can also exert immunosuppressive effects through interaction with natural Killer (NK) and T cells [14].

C3G (or RapGEF1) is a guanine nucleotide exchange factor (GEF) for Rap1 that regulates multiple cellular functions [21–24] through mechanisms dependent or independent of its GEF activity [25–27]. In cancer, C3G exerts different functions depending on tumor type and stage [23, 28, 29]. In HCC, C3G is upregulated [30] and plays a dual role promoting tumor growth, while inhibiting invasion.

C3G also induces megakaryocytic differentiation, pro-platelets formation [31] and regulates platelet biology [32–35]. Acting through Rap1b, C3G mediates signaling cascades triggered by several agonists to induce platelet activation, aggregation and thrombus formation. C3G also regulates platelet α–granule release via Rap1-dependent and independent mechanisms, favoring angiogenesis and metastasis in melanoma and lung cancer models [35, 36]. Based on C3G functions on platelets and the key role of platelets in liver fibrosis and HCC, we have evaluated how platelet C3G regulates these processes using genetically modified mouse models. Our results suggest that platelet C3G protects from liver fibrosis, favors chemically-induced tumor development and regulates immune response to liver damage.

MATERIAL AND METHODS

Genetically modified mice models

Transgenic mice overexpressing human full-length C3G (tgC3GFL) or C3G lacking the catalytic domain (tgC3GΔCat) in megakaryocytes and platelets, and a conditional megakaryocyte/platelet C3G knockout (PF4-C3GKO) mouse, previously described and characterized [31–36], were used. Each transgenic and knockout mouse has a different wt control, which may show behavior differences since they have different genetic backgrounds.

Induction of liver fibrosis and HCC associated with fibrosis

Liver fibrosis was induced with CCl_4 [37] and HCC associated with fibrosis with DEN (diethylnitrosamine) and CCl_4 [38] .

All animal experiments were carried out in compliance with the European Community Council Directive (2010/63/EU), following guidelines for animal research from Complutense University Ethical Committee, approved by Comunidad de Madrid (Spain) with references PROEX226.5/20 and PROEX176.0/24.

To analyze liver fibrosis dewaxed liver paraffin sections were stained with Picro-Sirius Red.

Isolation and analysis of non-parenchymal liver cells by flow cytometry

Non-parenchymal cells (NPCs) were isolated as previously described [39, 40].

Preparation of platelet-rich plasma, platelet stimulation with ADP and secretome generation

Blood collected in EDTA-pretreated tubes was centrifuged twice at 100g to obtain platelet-rich plasma (PRP). PRPs were centrifuged at 1300g to isolate platelets, which were stimulated with ADP and centrifuged at 2500g, getting the supernatant with the secretome.

Isolation and stimulation of peritoneal macrophages

Mice were treated with 3% thioglycolate and 4 days later the peritoneum fluid was aspirated to isolate macrophages. Cultured macrophages were stimulated with LPS (lipopolysaccharide) or platelet secretomes.

Wide proteomic analysis

PRPs´ protein extracts from PF4-C3GKO and wt mice treated with DEN+CCl_4 or the vehicle for 14 weeks were digested with trypsin and analyzed by liquid nano-chromatography coupled to a high-resolution mass spectrometer. Data were subjected to GO (Gene ontology) enrichment [41] and additional analyses.

Statistical analysis

Data are represented as the mean ± S.E.M. (n=3-8 mice). Unpaired Student's t-test, one-way or two-way ANOVA, followed by Tukey or Bonferroni multiple comparison test were used. Differences were considered significant when p value was $p \leq 0,05$.

See additional details in supplementary information.

RESULTS

Platelet C3G promotes platelet recruitment to the liver in response to CCl_4, protecting from fibrosis

Considering platelets´ involvement in CLD, regulating fibrosis and liver cancer [14, 15], and the important functions of C3G in platelets [32–36], we have explored the role of platelet C3G in CCl_4-induced liver fibrosis using genetically modified mouse models.

Treatment of mice with CCl_4 for 4 weeks led to similar collagen accumulation in livers from mice overexpressing C3GFL (tgC3GFL) or C3GΔCat (tgC3GΔCat) in platelets and wt (supplementary figure 1). However, after 8 weeks of treatment with CCl_4 less collagen was accumulated in livers from tgC3GFL compared to wt mice, while no differences between livers of tgC3GΔCat mice and their wt counterparts were found (figure 1A, supplementary figure 2A and supplementary table 2). In contrast, in PF4-C3GKO mice treated with CCl_4 for 8 weeks, collagen accumulation in the liver was significantly higher than in wt animals (figure 1A). Similarly, liver α-SMA levels, which

increased in response to CCl_4 (8 weeks) in mice from all genotypes, were lower in tgC3GFL, reaching the highest levels in PF4-C3GKO mice (figure 1B and supplementary figure 2B), which resulted in an increased activity of ALT (alanine amino transferase) and AST (aspartate amino transferase), indicative of liver damage (supplementary figure 3). This suggests that platelet C3G protects against liver fibrosis and chronic damage after CCl_4 treatment.

Next, we analyzed liver platelets. Figure 1C shows higher number of platelets ($CD41^+$) in livers from untreated tgC3GFL or tgC3GΔCat mice than in their wt counterparts. However, treatment with CCl_4 for 8 weeks only increased liver platelets in wt mice. In agreement with this, the number of liver platelets in PF4-C3GKO mice did not increase in response to CCl_4, remaining lower than in wt animals. This indicates that platelet C3G overexpression promotes platelet recruitment to the liver, even in untreated mice, while deletion of C3G in platelets prevents this recruitment in response to CCl_4.

Macrophages contribute to HSC activation and progression of liver fibrosis [42]. Therefore, we quantified liver macrophages (F4/80+). Untreated tgC3GFL and tgC3GΔCat mice had more liver macrophages (figure 1D), which decreased upon treatment with CCl_4 for 8 weeks in tgC3GFL mice, remaining unchanged in tgC3GΔCat animals. Moreover, the increase in liver macrophages induced by CCl_4 in wt mice was impaired in PF4-C3GKO animals. All this suggests that the number of liver macrophages is regulated by platelet C3G.

Different liver cell types, recruited immune cells, and platelets can secrete growth factors, cytokines and chemokines that regulate liver fibrosis. Hence, we evaluated the liver expression of some of them after 4- and 8-weeks treatment with CCl_4. *Hgf* mRNA was increased in livers from untreated tgC3GFL compared to wt mice at 4 weeks, showing a tendency to decrease upon CCl_4 treatment. However, no changes were found in tgC3GΔCat mice (supplementary figure 4). Curiously, *Il6* mRNA levels were upregulated in livers from untreated tgC3GFL and tgC3GΔCat mice, and *Il1b* mRNA was more expressed in livers from untreated tgC3GΔCat mice, decreasing after CCl_4 treatment for 4 weeks (supplementary figure 4). After 8 weeks of treatment with CCl_4 no significant differences in their expression between genotypes were found, except for the increase in *Il6* mRNA detected in livers from tgC3GFL mice (supplementary figure 5). Additionally, *Hgf* mRNA expression was reduced in PF4-C3GKO livers, increasing upon CCl_4 treatment (8 weeks). Since changes in these mRNAs were not significant in most cases, we determined IL-1β, IL-6 and CCL2 protein levels in the liver under these conditions. IL-1β protein levels decreased in livers from tgC3GFL mice as compared to their wt counterparts while pro-IL-1β remained unchanged. IL-6 levels increased in livers from tgC3GFL mice treated with CCl_4 and in untreated C3GΔCat mice when compared with their corresponding wt counterparts, while a reduction was observed in PF4-C3GKO mice (figure 2A and supplementary figure 6). No changes between genotypes were observed in CCL2 in response to CCl_4.

Platelet C3G regulates early liver immune response to CCl_4, increasing macrophage activation

Although platelet C3G seems to protect against liver fibrosis induced by CCl_4, we only detected limited changes in the expression of potential regulatory factors at either 4 or 8 weeks when comparing the different genotypes. Early changes in cytokines and chemokines (e.g. CXCL4) and the subsequent platelet recruitment are important to induce fibrosis and to recruit immune cells to the liver upon CCl_4 treatment [43]. Hence, we studied the acute response to CCl_4, determining the expression of IL-6, IL-1β, CCL2 and CXCL4 after a short-term treatment (24h) with CCl_4 in mice from all genotypes. Upon this short CCl_4 treatment, *Il6* mRNA levels were only significantly increased in livers from

PF4-C3GKO compared to wt mice, and CCl_4-induced *Il1b* mRNA expression was enhanced in tgC3GFL mice (Figure 2B). *Ccl2* mRNA expression was also accentuated in livers from tgC3GFL and PF4-C3GKO mice treated with CCl_4, while no differences between genotypes were observed in *Cxcl4* (Figure 2B). In most cases, the expression of these cytokines was similar in wt and tgC3GΔCat mice in response to CCl_4 (Figure 2B). Moreover, the analysis of IL-6, IL-1β and CCL2 protein levels under these conditions only revealed changes in IL-6 (figure 2C and supplementary figure 7). IL-6 levels increased more in livers from tgC3GFL mice treated with CCl_4 (24h) when compared to wt mice, although in all genotypes a rise was observed (figure 2C and supplementary figure 7).

Early changes in the immune cell populations induced by cytokines and other regulatory signals, some of them secreted by platelets, are relevant for chronic liver damage response [2, 13, 40]. Therefore, based on genotype-dependent differences in the number of liver macrophages after chronic CCl_4 treatment (figure 1D), liver macrophages and platelets, and serum ALT and AST activities were analyzed after CCl_4 treatment for 24h. Whereas the increase in serum ALT and AST activities induced by CCl_4 was similar in tgC3GFL and tgC3GΔCat compared to their wt mice, AST activity was higher in PF4-C3GKO than in wt mice (supplementary figure 8A). However, CCl_4 induced a similar recruitment of platelets to the liver in all genotypes (supplementary figure 8B), and liver macrophages remained unchanged or tended to decrease regardless of genotype (supplementary figure 8C). Therefore, to further understand the behavior of immune cells, a detailed analysis of immune cells was performed after 48h of CCl_4 treatment only in PF4-C3GKO mice and their corresponding wt counterparts. Upon CCl_4 treatment for 48h the number of active macrophages only increased in the liver of wt mice (figure 3A), while early recruited monocytes raised in PF4-C3GKO mice. On the other hand, monocyte-derived macrophages increased in the liver of both wt and PF4-C3G-KO mice treated with CCl_4 for 48h, reaching higher levels in PF4-C3GKO mice. Additionally, the number of lymphocytes and, specifically, helper T lymphocytes decreased after CCl_4 treatment for 48h only in wt mice (figure 3A). In contrast, cytotoxic lymphocytes did not change under any condition or genotype (figure 3A). On the other hand, the number of neutrophils was higher in the liver of untreated wt animals compared to PF4-C3GKO mice and decreased after CCl_4 treatment for 48h only in wt mice. However, the number of cytotoxic NK cells was significantly higher in livers from untreated PF4-C3GKO mice, decreasing upon CCl_4 treatment, while increasing in wt mice (figure 3A); whereas the number of helper NK cells decreased after CCl_4 treatment only in wt mice. Therefore, CD4+/CD8+ NKT ratio increased in livers from PF4-C3GKO mice treated with CCl4 for 48h.

All these data indicate that the early immune response to CCl_4 is altered in the liver of mice lacking C3G in platelets, being remarkable the reduced macrophage activation and the enhanced monocyte/macrophage recruitment.

To better understand how platelet C3G regulate macrophage phenotype, isolated macrophages were stimulated with secretomes from ADP-activated wt and PF4-C3GKO platelets, or LPS, an inducer of a pro-inflammatory phenotype. As expected, *Nos2* mRNA (encoding iNOS) was markedly induced by LPS and to a lesser extent by platelet secretomes, reaching higher levels with PF4-C3GKO-derived secretomes (figure 3B). Besides, *Arg1* mRNA expression (anti-inflammatory phenotype marker) tended to be higher upon stimulation with secretomes from wt platelets, and *Cd163* mRNA (anti-inflammatory phenotype marker) levels remained unchanged in all conditions (figure 3B). These data suggest that PF4-C3GKO platelets secrete factors that may favor a pro-inflammatory macrophage phenotype.

Deletion of C3G in platelets exacerbates liver fibrosis, while restraining hepatocarcinoma development induced by treatment with DEN plus CCl_4

Since platelet C3G seems to protect from liver fibrosis, we evaluated its function in a model of HCC associated with fibrosis induced by treatment with DEN and CCl_4 using PF4-C3GKO mice.

CCl_4 and DEN+CCl_4 induced a significantly higher collagen accumulation in livers from PF4-C3GKO compared to wt mice at 8 weeks (figure 1A, 4A and supplementary table 3). DEN+CCl_4 also induced visible liver tumors after 14 weeks of treatment in both wt and PF4-C3GKO mice (figure 4B and supplementary table 3). However, despite the lower fibrosis observed at 8 weeks in wt animals, the number of wt mice bearing more tumors was higher than in PF4-C3GKO animals (figure 4C), and tumors were larger (figure 4D) and less differentiated (according to their higher *Afp* expression (figure 4E).

Next, liver platelets were quantified. A significant increase in response to CCl_4 and DEN+CCl_4 was found only in wt mice at 8 and 14 weeks, especially in CCl_4 treatment (figure 2C and 4F). However, no changes were detected upon DEN treatment.

The expression of CLD regulatory factors was also studied. The mRNA levels of *Cxcl4*, a chemokine important in fibrosis [43], increased in livers from wt and PF4-C3GKO mice treated with DEN+CCl_4 for 8 weeks, but differences were only significant in wt animals, probably because of the higher basal levels found in PF4-C3GKO livers (figure 4G). Curiously, at 14 weeks, *Cxcl4* mRNA expression decreased in PF4-C3GKO livers in response to all treatments, while it increased in wt animals, being significantly higher in wt mice treated with CCl_4 or DEN+CCl_4. On the other hand, *Cxcl7* mRNA levels only increased in livers from PF4-C3GKO mice upon treatment with DEN+CCl_4 (8 or 14 weeks) or DEN for 14 weeks (figure 4G). *Ccl2* mRNA levels were also increased in livers from PF4-C3GKO mice treated with DEN+CCl_4 for 8 weeks compared to wt animals (figure 4G), while the opposite was observed at 14 weeks.

Moreover, *Hgf* mRNA levels decreased in the liver of wt mice treated with DEN+CCl_4 for 8 weeks, while increased in PF4-C3GKO livers, being significantly higher than in wt animals (supplementary figure 9A). Additionally, *Tgfb1* mRNA levels decreased in livers from wt mice in response to all treatments (supplementary figure 9), remaining lower and unchanged in untreated PF4-C3GKO animals. No major changes in *Hgf* or *Tgfb1* mRNA levels were found after DEN+CCl_4 treatment for 14 weeks, and *Il6* mRNA expression remained unchanged under all conditions (supplementary figure 9A).

Considering all this, we can highlight that the fibrosis degree is not directly associated with the presence of less tumors of reduced size in PF4-C3GKO mice. The different patterns of *Cxcl4*, *Cxcl7* and *Ccl2* expression may explain the differences in fibrosis and tumor growth.

Liver immune response is modified by the absence of C3G in platelets in a model of hepatocarcinoma induced by DEN plus CCl_4

The differences in chemokines´ expression in livers from wt and PF4-C3GKO mice induced by DEN+CCl_4 could modulate the immune response during HCC development/progression. Therefore, different immune cell populations were analyzed in liver tissues.

Figure 5A shows a significant increase in the number of liver macrophages ($F4/80^+$ cells) in response to CCl_4 and DEN+CCl_4 at 8 weeks in both wt and PF4-C3GKO mice. However, while there were more macrophages in livers from wt animals treated with CCl_4, upon DEN+CCl_4 treatment more macrophages were detected in PF4-C3GKO livers. After 14 weeks of treatment, a tendency to decrease liver macrophages in DEN and DEN+CCl_4 treated wt mice was observed, while they increased in DEN+CCl_4-treated PF4-C3GKO mice. Moreover, the mRNA expression of the pro-inflammatory phenotype

marker, *Nos2*, diminished in livers from wt mice treated with DEN+CCl_4 for 8 weeks, remaining unaltered and significantly higher in the livers of PF4-C3GKO (figure 5B). The mRNA levels of another marker of pro-inflammatory macrophages, *Cd68*, increased in PF4-C3GKO mouse livers treated with DEN+CCl_4 for 8 weeks, reaching significantly higher levels than in wt animals. Accordingly, the marker of pro-tumoral macrophages, *Cd163,* decreased (supplementary figure 9B).

On the other hand, positive cells for CD11b (highly expressed in monocytes/monocytes-derived macrophages) tended to increase in livers from wt animals treated with CCl_4 for 8 weeks and in livers from PF4-C3GKO mice treated with DEN+CCl_4, reaching significantly higher levels than in wt animals (figure 5C). In contrast, after 14 weeks of treatment, $CD11b^+$ cells significantly increased in livers from wt mice treated with either CCl_4 or DEN+CCl_4, reaching higher levels than in PF4-C3GKO mice. Curiously, $CD11b^+$ liver cells decreased upon DEN treatment in both wt and PF4-C3GKO mice at 8 and 14 weeks.

Liver cells positive for Ly6G (highly expressed in mature/activated neutrophils) showed a different pattern than that of $CD11b^+$ cells. CCl_4 treatment induced an increase in Ly6G+ area in livers from wt animals at 8 and 14 weeks, while in PF4-C3GKO mice only at 14 weeks (figure 5D). In contrast, upon DEN+CCl_4 treatment for 8 weeks, $Ly6G^+$ area increased only in livers from PF4-C3GKO mice, and the opposite was observed at 14 weeks, while DEN treatment had no effect.

All these data indicate that mice lacking platelet C3G have a different inflammatory response to chronic CCl_4 treatment, which is more remarkable upon DEN+CCl_4 treatment. Notably, the number of macrophages (likely pro-inflammatory) is higher in PF4-C3GKO than in wt mice livers under this treatment.

Platelet proteomic profile is differentially regulated in mice lacking platelet C3G treated with DEN plus CCl_4

According to literature [14, 15], proteins differentially present in platelets from wt and PF4-C3GKO mice could be involved in the regulation of liver immune cells in CLD, controlling fibrosis and/or HCC development upon secretion. Therefore, we performed a wide proteomic analysis in PRP from untreated and DEN+CCl_4-treated mice at 14 weeks.

A total of 48 proteins were differentially present in PRPs from untreated PF4-C3GKO vs wt, and 177 proteins in DEN+CCl_4 treated mice, 11 in common to both conditions (supplementary figure 10A). Functional enrichment analyses (GO and KEGG databases) of identified up- and/or down-regulated proteins in PRPs from untreated or DEN+CCl_4-treated PF4-C3GKO vs wt mice (supplementary figures 10B-10E and 11A-11C) revealed their involvement in different biological functions. Among them, in PRPs from untreated PF4-C3GKO mice it is remarkable the upregulation of proteins acting in stress response, catabolic processes, motility, defense response, endocytosis, proteolysis regulation, inflammatory response and actin filament polymerization pathways. Immune system proteins were downregulated in these PRPs (supplementary figure 10B). In addition, in PRPs from DEN+CCl_4 treated PF4-C3GKO mice vs wt, an upregulation of proteins involved in response to stimulus, chemicals and stress, and metabolic processes was observed. A downregulation of proteins from the immune system, inorganic substance, acute phase and inflammatory response, or wounding regulation pathways was also found in PRPs from DEN+CCl_4 treated PF4-C3GKO mice compared to wt (supplementary figure 10C). Additional analyses pointed to the regulation of more specific functional pathways such as platelet activation, adhesion and aggregation (supplementary figure 11A-11C), functions previously shown to be regulated by C3G [32, 34]. This confirms the validity of this study. We also found proteins implicated

in integrin signaling, actin cytoskeleton regulation, cell migration or immune response, among other processes regulated by C3G-Rap1 [34].

Among the proteins differentially present in PRPs from PF4-C3GKO vs wt mice treated with DEN+CCl_4, we found upregulation of Rap1a/b, GPV, CXCL4, α2 and β1 integrin, LECT2, Syntaxin 17, Rasa3, IGF1, Serpin b1, Arg1, BMP1, CXCL7 or Thbs1 (figure 6A-6B; supplementary figure 12A and 12B). Others were downregulated such as IGFBP2, Syntaxin 11 (Stx11), Ngp, Saa2, Fibulin 5, Serpin 1c, SOD1, Fibronectin or SOD3. In PRPs from untreated PF4-C3GKO vs wt mice (supplementary figure 12A-12B), examples of proteins upregulated were Slamf1, Rack1, VASP, Serpin1c, Ngp, Saa2, Snap23 or Cdc42, while of those downregulated were Collagen A1, Plecktrin1, Serpin3k, Rasgrp2 (also named CALDAG-GEFI), L-selectin, α6 integrin, AFP, GP1bb or CD177.

CXCL7, GPV and Stx11 protein levels were analyzed by western-blot in platelets to validate the wide proteomic analysis (figure 6C). GPV and CXCL7 levels were higher in PF4-C3GKO than in wt platelets from untreated or treated mice with CCl_4, DEN or DEN+CCl_4. On the other hand, Stx11 levels were downregulated in platelets from PF4-C3GKO mice treated with DEN or DEN+CCl_4 compared to wt platelets. These results validate data from wide proteomic analysis.

Some of the proteins differentially regulated in PRPs from DEN+CCl_4 treated PF4-C3GKO mice might play a role regulating liver cancer growth and/or fibrosis, although other proteins secreted by platelets could be also relevant. For example, CD40L, released by ADP-activated platelets, has been recently uncovered as an anti-tumor signal in liver diseases [44]. Hence, we determined its levels in the secretome of wt and PF4-C3GKO platelets stimulated with ADP. Figure 6D shows a tendency to increase CD40L release by PF4-C3GKO as compared to wt platelets. Therefore, it could contribute to decrease liver tumor growth.

Discussion

Platelets are key players in CLD, regulating fibrosis and liver cancer. However, their functions and the underlying mechanisms need to be further characterized since opposite roles for platelets have been described [14, 44–46]. Hence, based on the relevance of C3G protein as a regulator of platelet activation, spreading, secretion and other non-hemostatic functions [32–36], we have studied the role of platelet C3G in liver fibrosis and HCC associated with fibrosis in genetically modified mouse models. We describe here for the first time that platelet C3G promotes the recruitment of platelets to the liver in a context of fibrosis induced by CCl_4 or DEN+CCl_4 (figure 1C and 4F), exerting a protective role. The lower platelet recruitment to the liver in PF4-C3GKO mice might be due to a lower adhesion, owing to reduced surface levels of P-selectin and activated integrin αIIbβ3 [32, 34]. Moreover, actin polymerization alterations that prevent their spreading, favoring kiss-and-run exocytosis, could play a role [33]. It is also noticeable that both overexpression of full-length C3G and C3GΔCat increase liver platelets in the absence of treatment at 8 weeks (figure 1C), suggesting that C3G acts through both GEF dependent and independent mechanisms to facilitate platelet recruitment to the liver.

Platelets can exert both anti-fibrotic [15, 47, 48] or pro-fibrotic actions by secreting different regulatory factors through their interplay with liver and immune cells [13, 43, 49]. The higher expression of *Hgf* mRNA in the liver of untreated and CCl_4-treated wt compared to PF4-C3GKO mice after 8 weeks (supplementary figure 5) could facilitate an antifibrotic response [16]. IL-6, whose levels increased more in livers from tgC3GFL mice than from tgC3GΔCat or PF4-C3GKO mice when compared to their corresponding wt mice under these conditions (figure 2A), might also contribute to restrain fibrosis, limiting the differentiation of cirrhotic macrophages [50]. Moreover, the increased expression of *Ccl2* mRNA induced by DEN+CCl_4 at 8 weeks in livers from PF4-C3GKO

mice (figure 4G) might enhance monocyte recruitment and differentiation into macrophages, in agreement with previous studies on CLD, and patient data [51, 52]. Thus, upon liver damage, liver cells (hepatocytes, KCs and HSCs) and platelets, [8] secrete CCL2, promoting the generation of pro-inflammatory/fibrogenic macrophages that can induce HSC transdifferentiation into myofibroblast. Hence, CCL2 blockage improved liver fibrosis in mice [52]. Supporting this role of CCL2 in PF4-C3GKO mice, we found that thrombin-activated PF4-C3GKO platelets secrete more CCL2 than C3G transgenic platelets (supplementary figure 12C). Additionally, immune cells could contribute to enhance fibrosis. For example, the lower number of neutrophils present in the liver of untreated PF4-C3GKO mice (figure 3A) might facilitate fibrosis as specific subtypes of neutrophils can degrade collagen [53].

Our data also suggest that C3G effects on fibrosis would be, at least, partially dependent on its GEF activity, as transgenic overexpression of C3G lacking the catalytic domain in platelets did not protect from fibrosis as it did C3GFL overexpression (figure 1A-1B). However, considering the increased liver fibrosis found in PF4-C3GKO mice treated with CCl_4 (8 weeks) compared to tgC3GΔCat animals, GEF independent mechanisms may contribute to the antifibrotic effect of platelet C3G.

CXCL4 (PF4), synthesized and secreted by platelets and cancer cells can also promote CCl_4-induced liver fibrosis in mice [43]. The tendency to increase *Cxcl4* mRNA levels in livers from PF4-C3GKO compared to wt mice treated with CCl_4 or DEN+CCl_4 for 8 weeks (figure 4G) supports it. CXCL4 protein levels were also upregulated in platelets from PF4-C3GKO compared to wt mice treated with DEN+CCl_4 for 14 weeks (figure 6A-6B). Moreover, thrombin-activated C3GKO platelets secrete more CXCL4 than C3G transgenic platelets (supplementary figure 12C).

Curiously, despite the higher fibrosis observed in mice lacking C3G in platelets, liver tumors were smaller (figure 4B) and more differentiated (figure 4E). The higher levels of IL-6 present in the liver of wt vs PF4-C3GKO mice after treatment with CCl_4 for 8 weeks could support it (figure 2A), as persistent activation of IL-6 signaling pathway promotes tumor growth [54]. It is also worth mentioning that, although 90% of HCC cases develop in a context of CLD [2], specific somatic mutations occurring in hepatocyte premalignant lesions of patients with liver cirrhosis can promote liver regeneration rather than HCC [55]. In addition, during regenerative response to chronic liver damage, pre-malignant nodules can be surrounded by fibrotic septa, limiting tumor cell dissemination [56]. Hence, collagen accumulation in the liver correlates with less and smaller tumors in some studies [57], as it occurs in PF4-C3GKO mice treated with DEN+CCl_4. ECM stiffness also plays a role. Hence, a higher matrix stiffness promotes a stem-like phenotype that could favor HCC development [58].

Concerning platelet function in HCC, a high platelet count has been associated with poor prognosis of HCC patients [18, 20]. Hence, antiplatelet therapy reduces HCC risk in patients with viral hepatitis [19, 45] and HCC development in a chronic hepatitis B mouse model, while having no effect on chemically-induced HCC [59]. Tumor associated platelets can protect HCC cells from immune cell recognition, and by the release of their granule content facilitate their proliferation and transendothelial migration [15, 60]. Platelets also induce proliferation of liver sinusoidal endothelial cells and hepatocytes, liver regeneration and immune cell recruitment [14]. Therefore, the presence of more platelets in livers from wt compared to PF4-C3GKO mice treated with DEN+CCl_4 would explain the increased size of liver tumors and the differences in liver immune cell populations. Concerning this, C3G regulates the selective secretion of components from platelet granules [33, 35, 36], promoting tumor growth and metastasis in lung cancer and melanoma mouse models. In this regard, Syntaxin 11, which is required for platelet secretion and extension [61], and interacts with C3G [33], is downregulated in PRPs from

PF4-C3GKO mice treated with DEN+CCl_4 for 14 weeks (figure 6A-C). This further supports the implication of C3G regulated platelet secretion**.** In this line, the upregulation of CXCL7 protein in PRPs from PF4-C3GKO treated with DEN+CCl_4 for 14 weeks (figure 6A-6C) could result in its higher secretion, although different immune cells can also express CXCL7 [62]. In cholangiocarcinoma, its levels increase [63], promoting proliferation and invasion [64]. High CXCL7 levels are also associated with inflammation and poor prognosis in hepatoblastoma [65]. In contrast, lower *Cxcl7* mRNA levels were detected in HCC [66]. In this study, the high levels of CXCL7 in PF4-C3GKO platelets and its high expression in livers from DEN+CCl_4 treated PF4-C3GKO mice do not correlate with HCC progression. Hence, CXCL7 could protect from HCC development/progression through regulation of immune cells.

On the other hand, the higher release of CD40L by PF4-C3GKO platelets stimulated with ADP (Figure 6D) could contribute to the anti-tumor effect based on the proved platelet-mediated enhancement of CD8+T cell-dependent anti-tumor immune response in MAFLD (formerly NAFLD) mouse models through P2Y12-induced CD40L release [44]. Hence, platelet C3G through finely tuning the secretion of components from platelet granules could regulate HCC by controlling the immune response. In this regard, the higher number of macrophages (likely pro-inflammatory) and $CD11b^+$ cells (monocytes/monocyte-derived macrophages) (figure 5C) in livers from DEN+CCl_4 treated PF4-C3GKO mice for 8 weeks might facilitate an antitumor response by releasing pro-inflammatory and repair-associated cytokines [8]. In addition, changes in $Ly6G^+$ population (likely neutrophils) upon DEN+CCl_4 treatment (figure 5D) might play either a beneficial or deleterious role [67] depending on their subtype [68]: anti-tumoral N1 tumor associated neutrophils (TANs) or pro-tumoral N2 TANs [67, 69]. Hence, the larger Ly6G+ area detected in livers from wt compared to PF4-C3GKO mice treated with DEN+CCl_4 for 14 weeks and the higher *Ccl2* mRNA expression might support a higher presence of N2 TANs that might secrete CCL2, favoring tumor growth.

Platelet C3G could also regulate HCC and fibrosis through LECT2, whose expression is downregulated in HCC, favoring HCC development and the accumulation of immature inflammatory monocytes with immunosuppressive characteristics [70]. LECT2 can also enhance fibrosis [71]. Therefore, LECT2 upregulation in PRPs from DEN+CCl_4-treated PF4-C3GKO mice could reduce HCC development, while increasing fibrosis.

In conclusion, in this work we have uncovered a new function of the protein C3G from platelets in a model of liver fibrosis and HCC associated with fibrosis. While platelet C3G protects against fibrosis, it accelerates HCC development and/or progression (see scheme in supplementary figure 13). All this might be mediated by changes in the liver inflammatory response (supplementary tables 4 and 5) and the expression of growth factors, cytokines and chemokines dependent on platelet C3G.

Acknowledgements

We thank Mª Luisa Hernáez from *Universidad Complutense de Madrid* (UCM) Proteomics Unit for her very helpful assistance in the analysis of proteomic data.
"The mass spectrometry proteomics data have been deposited to the ProteomeXchange Consortium via the PRIDE [72] partner repository with the dataset identifier PXD050819 and 10.6019/PXD050819".

Funding
This work was supported by grants from the Spanish Ministry of Economy and Competitiveness and Science, Innovation and Universities [PID2022-137717OB-C21 to

AP/AMC; PID2019-104143RB-C22 to AP; PID2022-137717OB-C22 to CG; PID2019-104143RB-C21 to CG; PID2019-104991RB-I00 and PID2022-136959OB-I00 to PB, PID2020-117650RA-I00 and CNS2023-144109 to AG-U, PID-2021-122766OB-100 to AVM and funded by MICIU/AEI/10.13039/501100011033]. All funding was cosponsored by the European “ERDF A way of making Europe”. CB was supported by PID2019-104143RB-C22 grant. NP was a recipient of FPU fellowship from Spanish Ministry of Education. MI is supported by a predoctoral contract from *Comunidad de Madrid*. MC is a recipient of a predoctoral contract from UCM.

Author contribution statement

CB, MI-G, NP, CF-I, PV MC-R and JM were involved in methodology, data acquisition, analysis and/or interpretation. MR-F, CS and SM contributed to data analysis and reviewed the manuscript. SC obtained and analyzed proteomic data. AMC was involved in data acquisition, supervision, and discussion of the results. AMV, AMC, AG-U, PB, CG and AP acquired funding. AP and PB conceived and designed the study and supervised the experiments. AP wrote the original draft of the manuscript. PB, CG and AG-U were involved in supervision, discussion of results and critically reviewing the manuscript. All authors read and approved the final manuscript.

References

[1] Delgado ME, Cárdenas BI, Farran N, et al. Metabolic Reprogramming of Liver Fibrosis. *Cells* 2021; **10**: 3604.

[2] Llovet JM, Kelley RK, Villanueva A, et al. Hepatocellular carcinoma. *Nat Rev Dis Primers* 2021; **7**: 6.

[3] Affo S, Yu L-X, Schwabe RF. The Role of Cancer-Associated Fibroblasts and Fibrosis in Liver Cancer. *Annual Review of Pathology: Mechanisms of Disease* 2017; **12**: 153–186.

[4] Sánchez PS, Rigual M del M, Djouder N. Inflammatory and Non-Inflammatory Mechanisms Controlling Cirrhosis Development. *Cancers (Basel)* 2021; **13**: 5045.

[5] Acharya P, Chouhan K, Weiskirchen S, et al. Cellular Mechanisms of Liver Fibrosis. *Front Pharmacol*; **12**. Epub ahead of print 6 May 2021. DOI: 10.3389/fphar.2021.671640.

[6] Kuwahara R, Kofman A V., Landis CS, et al. The hepatic stem cell niche: Identification by label-retaining cell assay. *Hepatology* 2008; **47**: 1994–2002.

[7] Cuesta ÁM, Palao N, Bragado P, et al. New and Old Key Players in Liver Cancer. *Int J Mol Sci* 2023; **24**: 17152.

[8] Triantafyllou E, Woollard KJ, McPhail MJW, et al. The Role of Monocytes and Macrophages in Acute and Acute-on-Chronic Liver Failure. *Front Immunol* 2018; **9**: 2948.

[9] Delgado A, Guddati AK. Clinical endpoints in oncology - a primer. *Am J Cancer Res* 2021; **11**: 1121–1131.

[10] Ramachandran P, Dobie R, Wilson-Kanamori JR, et al. Resolving the fibrotic niche of human liver cirrhosis at single-cell level. *Nature* 2019; **575**: 512–518.

[11] Cogliati B, Yashaswini CN, Wang S, et al. Friend or foe? The elusive role of hepatic stellate cells in liver cancer. *Nat Rev Gastroenterol Hepatol* 2023; **20**: 647–661.

[12] Hao X, Sun G, Zhang Y, et al. Targeting Immune Cells in the Tumor Microenvironment of HCC: New Opportunities and Challenges. *Front Cell Dev Biol* 2021; **9**: 775462.

[13] Malehmir M, Pfister D, Gallage S, et al. Platelet GPIbα is a mediator and potential interventional target for NASH and subsequent liver cancer. *Nat Med* 2019; **25**: 641–655.

[14] Pavlovic N, Rani B, Gerwins P, et al. Platelets as Key Factors in Hepatocellular Carcinoma. *Cancers (Basel)* 2019; **11**: 1022.

[15] Mussbacher M, Brunnthaler L, Panhuber A, et al. Till Death Do Us Part—The Multifaceted Role of Platelets in Liver Diseases. *Int J Mol Sci* 2021; **22**: 3113.

[16] Murata S, Maruyama T, Nowatari T, et al. Signal transduction of platelet-induced liver regeneration and decrease of liver fibrosis. *Int J Mol Sci* 2014; **15**: 5412–25.

[17] Li S, Lu Z, Wu S, et al. The dynamic role of platelets in cancer progression and their therapeutic implications. *Nat Rev Cancer* 2024; **24**: 72–87.

[18] Liu P, Hsu C, Su C, et al. Thrombocytosis is associated with worse survival in patients with hepatocellular carcinoma. *Liver International* 2020; **40**: 2522–2534.

[19] Simon TG, Duberg A-S, Aleman S, et al. Association of Aspirin with Hepatocellular Carcinoma and Liver-Related Mortality. *New England Journal of Medicine* 2020; **382**: 1018–1028.

[20] Scheiner B, Kirstein M, Popp S, et al. Association of Platelet Count and Mean Platelet Volume with Overall Survival in Patients with Cirrhosis and Unresectable Hepatocellular Carcinoma. *Liver Cancer* 2019; **8**: 203–217.

[21] Maia V, Sanz M, Gutierrez-Berzal J, et al. C3G silencing enhances STI-571-induced apoptosis in CML cells through p38 MAPK activation, but it antagonizes STI-571 inhibitory effect on survival. *Cell Signal* 2009; **21**: 1229–1235.

[22] Gutiérrez-Uzquiza Á, Arechederra M, Molina I, et al. C3G down-regulates p38 MAPK activity in response to stress by Rap-1 independent mechanisms: Involvement in cell death. *Cell Signal* 2010; **22**: 533–542.

[23] Priego N, Arechederra M, Sequera C, et al. C3G knock-down enhances migration and invasion by increasing Rap1-mediated p38α activation, while it impairs tumor growth through p38α-independent mechanisms. *Oncotarget* 2016; **7**: 45060–45078.

[24] Palao N, Sequera C, Cuesta ÁM, et al. C3G down-regulation enhances pro-migratory and stemness properties of oval cells by promoting an epithelial-mesenchymal-like process. *Int J Biol Sci* 2022; **18**: 5873–5884.

[25] Guerrero C, Fernandez-Medarde A, Rojas J, et al. Transformation suppressor activity of C3G is independent of its CDC25-homology domain. *Oncogene* 1998; **16**: 613–624.

[26] Martín-Encabo S, Santos E, Guerrero C. C3G mediated suppression of malignant transformation involves activation of PP2A phosphatases at the subcortical actin cytoskeleton. *Exp Cell Res* 2007; **313**: 3881–3891.

[27] Carabias A, Gómez-Hernández M, de Cima S, et al. Mechanisms of autoregulation of C3G, activator of the GTPase Rap1, and its catalytic deregulation in lymphomas. *Sci Signal*; **13**. Epub ahead of print September 2020. DOI: 10.1126/scisignal.abb7075.

[28] Gutiérrez-Berzal J, Castellano E, Martín-Encabo S, et al. Characterization of p87C3G, a novel, truncated C3G isoform that is overexpressed in chronic myeloid leukemia and interacts with Bcr-Abl. *Exp Cell Res* 2006; **312**: 938–948.

[29] Manzano S, Gutierrez-Uzquiza A, Bragado P, et al. C3G downregulation induces the acquisition of a mesenchymal phenotype that enhances aggressiveness of glioblastoma cells. *Cell Death Dis* 2021; **12**: 348.

[30] Sequera C, Bragado P, Manzano S, et al. C3G is upregulated in hepatocarcinoma, contributing to tumor growth and progression and to HGF/MET pathway activation. *Cancers (Basel)* 2020; **12**: 1–22.

[31] Ortiz-Rivero S, Baquero C, Hernández-Cano L, et al. C3G, through its GEF activity, induces megakaryocytic differentiation and proplatelet formation. *Cell Commun Signal* 2018; **16**: 101.

[32] Gutiérrez-Herrero S, Maia V, Gutiérrez-Berzal J, et al. C3G transgenic mouse models with specific expression in platelets reveal a new role for C3G in platelet clotting through its GEF activity. *Biochim Biophys Acta Mol Cell Res* 2012; **1823**: 1366–1377.

[33] Fernández-Infante C, Hernández-Cano L, Herranz Ó, et al. Platelet C3G: a key player in vesicle exocytosis, spreading and clot retraction. *Cellular and Molecular Life Sciences* 2024; **81**: 84.

[34] Gutiérrez-Herrero S, Fernández-Infante C, Hernández-Cano L, et al. C3G contributes to platelet activation and aggregation by regulating major signaling pathways. *Signal Transduct Target Ther* 2020; **5**: 29.

[35] Hernández-Cano L, Fernández-Infante C, Herranz Ó, et al. New functions of C3G in platelet biology: Contribution to ischemia-induced angiogenesis, tumor metastasis and TPO clearance. *Front Cell Dev Biol* 2022; **10**: 1026287.

[36] Martín-Granado V, Ortiz-Rivero S, Carmona R, et al. C3G promotes a selective release of angiogenic factors from activated mouse platelets to regulate angiogenesis and tumor metastasis. *Oncotarget* 2017; **8**: 110994–111011.

[37] Paquet KJ, Kamphausen U. The carbon-tetrachloride-hepatotoxicity as a model of liver damage. First report: Long-time biochemical changes. *Acta Hepatogastroenterol (Stuttg)* 1975; **22**: 84–8.

[38] Uehara T, Pogribny IP, Rusyn I. The DEN and CCl4 -Induced Mouse Model of Fibrosis and Inflammation-Associated Hepatocellular Carcinoma. *Curr Protoc Pharmacol* 2014; **66**: 14.30.1-14.30.10.

[39] González-Rodríguez Á, Valdecantos MP, Rada P, et al. Dual role of protein tyrosine phosphatase 1B in the progression and reversion of non-alcoholic steatohepatitis. *Mol Metab* 2018; **7**: 132–146.

[40] Brea R, Valdecantos P, Rada P, et al. Chronic treatment with acetaminophen protects against liver aging by targeting inflammation and oxidative stress. *Aging* 2021; **13**: 7800–7827.

[41] Kolberg L, Raudvere U, Kuzmin I, et al. gprofiler2 -- an R package for gene list functional enrichment analysis and namespace conversion toolset g:Profiler. *F1000Res* 2020; **9**: 709.

[42] Pradere J-P, Kluwe J, De Minicis S, et al. Hepatic macrophages but not dendritic cells contribute to liver fibrosis by promoting the survival of activated hepatic stellate cells in mice. *Hepatology* 2013; **58**: 1461–1473.

[43] Zaldivar MM, Pauels K, von Hundelshausen P, et al. CXC chemokine ligand 4 (Cxcl4) is a platelet-derived mediator of experimental liver fibrosis. *Hepatology* 2010; **51**: 1345–1353.

[44] Ma C, Fu Q, Diggs LP, et al. Platelets control liver tumor growth through P2Y12-dependent CD40L release in NAFLD. *Cancer Cell* 2022; **40**: 986-998.e5.

[45] Lee M, Chung GE, Lee J, et al. Antiplatelet therapy and the risk of hepatocellular carcinoma in chronic hepatitis B patients on antiviral treatment. *Hepatology* 2017; **66**: 1556–1569.

[46] Ramadori P, Klag T, Malek NP, et al. Platelets in chronic liver disease, from bench to bedside. *JHEP Reports* 2019; **1**: 448–459.

[47] Takahashi K. Human platelets inhibit liver fibrosis in severe combined immunodeficiency mice. *World J Gastroenterol* 2013; **19**: 5250.

[48] Ikeda N, Murata S, Maruyama T, et al. Platelet-derived adenosine 5′-triphosphate suppresses activation of human hepatic stellate cell: *In vitro* study. *Hepatology Research* 2012; **42**: 91–102.

[49] Chauhan A, Adams DH, Watson SP, et al. Platelets: No longer bystanders in liver disease. *Hepatology* 2016; **64**: 1774–1784.

[50] Buonomo EL, Mei S, Guinn SR, et al. Liver stromal cells restrict macrophage maturation and stromal IL-6 limits the differentiation of cirrhosis-linked macrophages. *J Hepatol* 2022; **76**: 1127–1137.

[51] Karlmark KR, Weiskirchen R, Zimmermann HW, et al. Hepatic recruitment of the inflammatory Gr1+ monocyte subset upon liver injury promotes hepatic fibrosis. *Hepatology* 2009; **50**: 261–274.

[52] Baeck C, Wei X, Bartneck M, et al. Pharmacological inhibition of the chemokine C-C motif chemokine ligand 2 (monocyte chemoattractant protein 1) accelerates liver fibrosis regression by suppressing Ly-6C+ macrophage infiltration in mice. *Hepatology* 2014; **59**: 1060–1072.

[53] Saijou E, Enomoto Y, Matsuda M, et al. Neutrophils alleviate fibrosis in the CCl4-induced mouse chronic liver injury model. *Hepatol Commun* 2018; **2**: 703–717.

[54] Schmidt-Arras D, Rose-John S. IL-6 pathway in the liver: From physiopathology to therapy. *J Hepatol* 2016; **64**: 1403–1415.

[55] Zhu M, Lu T, Jia Y, et al. Somatic Mutations Increase Hepatic Clonal Fitness and Regeneration in Chronic Liver Disease. *Cell* 2019; **177**: 608-621.e12.

[56] Bhattacharjee S, Hamberger F, Ravichandra A, et al. Tumor restriction by type I collagen opposes tumor-promoting effects of cancer-associated fibroblasts. *J Clin Invest*; **131**. Epub ahead of print 1 June 2021. DOI: 10.1172/JCI146987.

[57] Baglieri J, Zhang C, Liang S, et al. Nondegradable Collagen Increases Liver Fibrosis but Not Hepatocellular Carcinoma in Mice. *Am J Pathol* 2021; **191**: 1564–1579.

[58] Wei J, Yao J, Yang C, et al. Heterogeneous matrix stiffness regulates the cancer stem-like cell phenotype in hepatocellular carcinoma. *J Transl Med* 2022; **20**: 555.

[59] Sitia G, Aiolfi R, Di Lucia P, et al. Antiplatelet therapy prevents hepatocellular carcinoma and improves survival in a mouse model of chronic hepatitis B. *Proc Natl Acad Sci U S A* 2012; **109**: E2165-72.

[60] Tesfamariam B. Involvement of platelets in tumor cell metastasis. *Pharmacol Ther* 2016; **157**: 112–119.

[61] Ye S, Karim ZA, Al Hawas R, et al. Syntaxin-11, but not syntaxin-2 or syntaxin-4, is required for platelet secretion. *Blood* 2012; **120**: 2484–2492.

[62] Brown AJ, Sepuru KM, Sawant K V, et al. Platelet-Derived Chemokine CXCL7 Dimer Preferentially Exists in the Glycosaminoglycan-Bound Form: Implications for Neutrophil-Platelet Crosstalk. *Front Immunol* 2017; **8**: 1248.

[63] Wu Q, Tu H, Li J. Multifaceted Roles of Chemokine C-X-C Motif Ligand 7 in Inflammatory Diseases and Cancer. *Front Pharmacol* 2022; **13**: 914730.

[64] Guo Q, Jian Z, Jia B, et al. CXCL7 promotes proliferation and invasion of cholangiocarcinoma cells. *Oncol Rep* 2017; **37**: 1114–1122.

[65] Guo F, Ru Q, Zhang J, et al. Inflammation factors in hepatoblastoma and their clinical significance as diagnostic and prognostic biomarkers. *J Pediatr Surg* 2017; **52**: 1496–1502.

[66] Zajkowska M, Mroczko B. Chemokines in Primary Liver Cancer. *Int J Mol Sci* 2022; **23**: 8846.

[67] Liu K, Wang F-S, Xu R. Neutrophils in liver diseases: pathogenesis and therapeutic targets. *Cell Mol Immunol* 2021; **18**: 38–44.

[68] Xue R, Zhang Q, Cao Q, et al. Liver tumour immune microenvironment subtypes and neutrophil heterogeneity. *Nature* 2022; **612**: 141–147.

[69] Finisguerra V, Di Conza G, Di Matteo M, et al. MET is required for the recruitment of anti-tumoural neutrophils. *Nature* 2015; **522**: 349–353.

[70] L'Hermitte A, Pham S, Cadoux M, et al. Lect2 Controls Inflammatory Monocytes to Constrain the Growth and Progression of Hepatocellular Carcinoma. *Hepatology* 2019; **69**: 160–178.

[71] Xu M, Xu H-H, Lin Y, et al. LECT2, a Ligand for Tie1, Plays a Crucial Role in Liver Fibrogenesis. *Cell* 2019; **178**: 1478-1492.e20.

[72] Perez-Riverol Y, Bai J, Bandla C, et al. The PRIDE database resources in 2022: a hub for mass spectrometry-based proteomics evidences. *Nucleic Acids Res* 2022; **50**: D543–D552.

Figure legends

Figure 1-Platelet C3G increases platelet recruitment to the liver and liver macrophages reducing fibrosis. Mice overexpressing full length C3G (tgC3GFL) or C3G lacking the catalytic domain (tgC3GΔCat), as well as those lacking C3G (PF4-C3GKO) in megakaryocytes and platelets and their corresponding wt counterparts were treated with CCl_4 or the vehicle (controls) for the indicated times. A) Analysis of collagen accumulation by Sirius Red staining in liver sections. Upper panels, representative microscope images; and lower panels, graphics showing quantification of positive areas (percentage) for each sample and the mean values ± S.E.M.. B) Analysis of α-SMA levels in liver sections. Upper panels, representative microscope images; and lower panels, graphics showing quantification of α-SMA positive areas (percentage) for each sample and the mean values ± S.E.M.. C) Immunohistochemical analysis of liver platelets detected with CD41 antibody. Upper panels, representative microscope images; and lower panels, graphics showing the number of CD41 positive cells/field for each condition and the mean values ± S.E.M.. D) Immunohistochemical analysis of liver macrophages detected with F4/80 antibody. Upper panels, representative microscope images; and lower panels, graphics showing the number of F4/80 positive cells/field for each condition and the mean values ± S.E.M.. *p≤0,05, **p≤0,01 and ***p≤0,001 compared as indicated (n=4-8). Scale bars: 20 μm.

Figure 2-Regulation of the expression of cytokines and chemokines by platelet C3G in response to chronic and acute treatment with CCl_4. Mice overexpressing full length C3G (tgC3GFL) or C3G lacking the catalytic domain (tgC3GΔCat), as well as those lacking C3G (PF4-C3GKO) in megakaryocytes and platelets and their corresponding wt counterparts were treated with CCl_4 or the vehicle (controls) for the indicated times. A) and C) Western-blot analysis of IL-1β (pro-form and mature IL-1β), IL-6 and CCL2 in liver extracts normalized with β-Actin. B) RT-qPCR analysis of *Il6*, *Il1b*, *Ccl2* and *Cxcl4* mRNA levels in liver samples. Histograms showing RQ mean values ± S.E.M. and the individual values of each sample. *p≤0,05, **p≤0,01 and ***p≤0,001 compared as indicated (n=3-8).

Figure 3-Platelet C3G regulates early liver immune response induced by CCl_4 and macrophage phenotype. A) Mice lacking C3G (PF4-C3GKO) in megakaryocytes and platelets and their corresponding wt counterparts were treated with CCl_4 or the vehicle (controls) for 48h. Isolated non-parenchymal liver cells were analyzed by flow cytometry to determine the proportion of different immune cells. Histograms show the percentage (mean values ± S.E.M.) of the different subpopulations of $CD45^+$ cells labelled as

indicated. n=4-7. *p≤0,05, **p≤0,01 and ***p≤0,001 compared as indicated (n=4-8). Scale bars: 20 μm. B) RT-qPCR analysis of *Nos2, Arg1 and Cd163* mRNA levels in macrophages treated with LPS, or secretomes from activated wt and PF4-C3GKO platelets. Histograms showing RQ mean values ± S.E.M. and the individual values of each sample (n=4).

Figure 4-Platelet C3G protects from fibrosis, while favors liver tumor growth. Mice lacking C3G (PF4-C3GKO) in megakaryocytes and platelets and their corresponding wt counterparts were treated with CCl_4, DEN, DEN+CCl_4 or vehicle (control) for the indicated times (8 or 14 weeks). A) Analysis of collagen accumulation by Sirius Red staining in liver sections. Upper panels, representative microscope images; and lower panels, graphics showing quantification of positive areas (percentage) for each sample and the mean values ± S.E.M.. B) Macroscopic (left panels) and microscopic hematoxylin&eosin (right panels) images of liver tumors induced by DEN+CCl_4 treatment and their corresponding controls. C) Histograms show the percentage of mice (mean values ± S.E.M.) with the indicated number of tumors. D) The graphic shows the area (mean values ± S.E.M.) occupied by tumors. E) RT-qPCR analysis of *Afp* mRNA levels in liver samples. Histograms showing RQ mean values ± S.E.M. and the individual values of each sample after 8 (left panel) or 14 weeks (right panel) of treatment. F) Immunohistochemical analysis of liver platelets detected with anti-CD41 antibody. Left panels, representative microscope images; and right panels, graphics showing the number of CD41 positive cells for each condition and the mean values ± S.E.M.. *p≤0,05, **p≤0,01 and ***p≤0,001 compared as indicated (n=4-8). Scale bars: 20 μm. G) RT-qPCR analysis of *Cxcl4, Cxcl7 and Ccl2* mRNA levels in liver samples. Histograms showing RQ mean values ± S.E.M. and the individual values of each sample after 8 (upper panel) or 14 weeks (lower panel) of treatment. *p≤0,05, **p≤0,01 and ***p≤0,001 compared as indicated (n=4-8). Scale bars: 20 μm.

Figure 5-Effect of platelet C3G on liver immune cells upon chemically induced liver cancer associated with fibrosis. Mice lacking C3G (PF4-C3GKO) in megakaryocytes and platelets and their corresponding wt counterparts were treated with CCl_4, DEN, DEN+CCl_4 or vehicle (control) for the indicated times (8 or 14 weeks). A) Immunohistochemical analysis of liver macrophages detected with F4/80 antibody. Left panels, representative microscope images; and right panels, graphics showing the number of F4/80 positive cells for each condition and the mean values ± S.E.M.. C) RT-qPCR analysis of mRNA levels of the markers of pro-inflammatory macrophages, *Nos2 and Cd68* in liver samples. Histograms showing RQ mean values ± S.E.M. and the individual values of each sample after 8 or 14 weeks of treatment as indicated. C) Immunohistochemical analysis of CD11b positive cells. Left panels, representative microscope images; and right panels, graphics showing the number of CD11b positive cells/field for each condition and the mean values ± S.E.M.. D) Immunohistochemical analysis of Ly6G positive cells. Left panels, representative microscope images; and right panels, graphics showing Ly6G positive area for each condition and the mean values ± S.E.M.. *p≤0,05, **p≤0,01 and ***p≤0,001 compared as indicated (n=4-8). Scale bars: 20 μm.

Figure 6-Deletion of C3G in platelets induces changes in the proteins present in platelet rich plasma upon chemically induced liver cancer associated with fibrosis. Mice lacking C3G (PF4-C3GKO) in megakaryocytes and platelets and their corresponding wt counterparts were treated with DEN+CCl_4 for 14 weeks. A wide proteomic analysis of platelet rich plasma (PRP) was performed and then, PRPs from

PF4-C3GKO mice were compared with wt ones. A) Volcano plot and B) bar graphic show proteins upregulated (in red), downregulated (in blue) or unchanged (in grey) in PF4-C3GKO vs wt PRPs. The names of some proteins are included. The -log10 of p value obtained from the applied statistical method is represented. C) Western-blot analysis of GPV, CXCL7 and Syntaxin 11 protein levels normalized with Rho-GDI or β-actin in PRPs from mice treated CCl_4, DEN, DEN+CCl_4 or vehicle (control) for 14 weeks. Quantification of band intensity vs Rho-GDI is shown. D) Western-blot analysis of CD40L in platelets and platelet secretome after activation of platelets with ADP normalized with Rho-GDI. Upper panels, representative western-blots of wt and PF4-C3GKO samples. Membrane was cut, which is indicated by the dashed line. Lower panel, histograms show the levels of CD40L in platelets and in secretomes (individual and mean values ± S.E.M.), expressed as fold increase of wt vs PF4-C3GKO values.

Figure 1

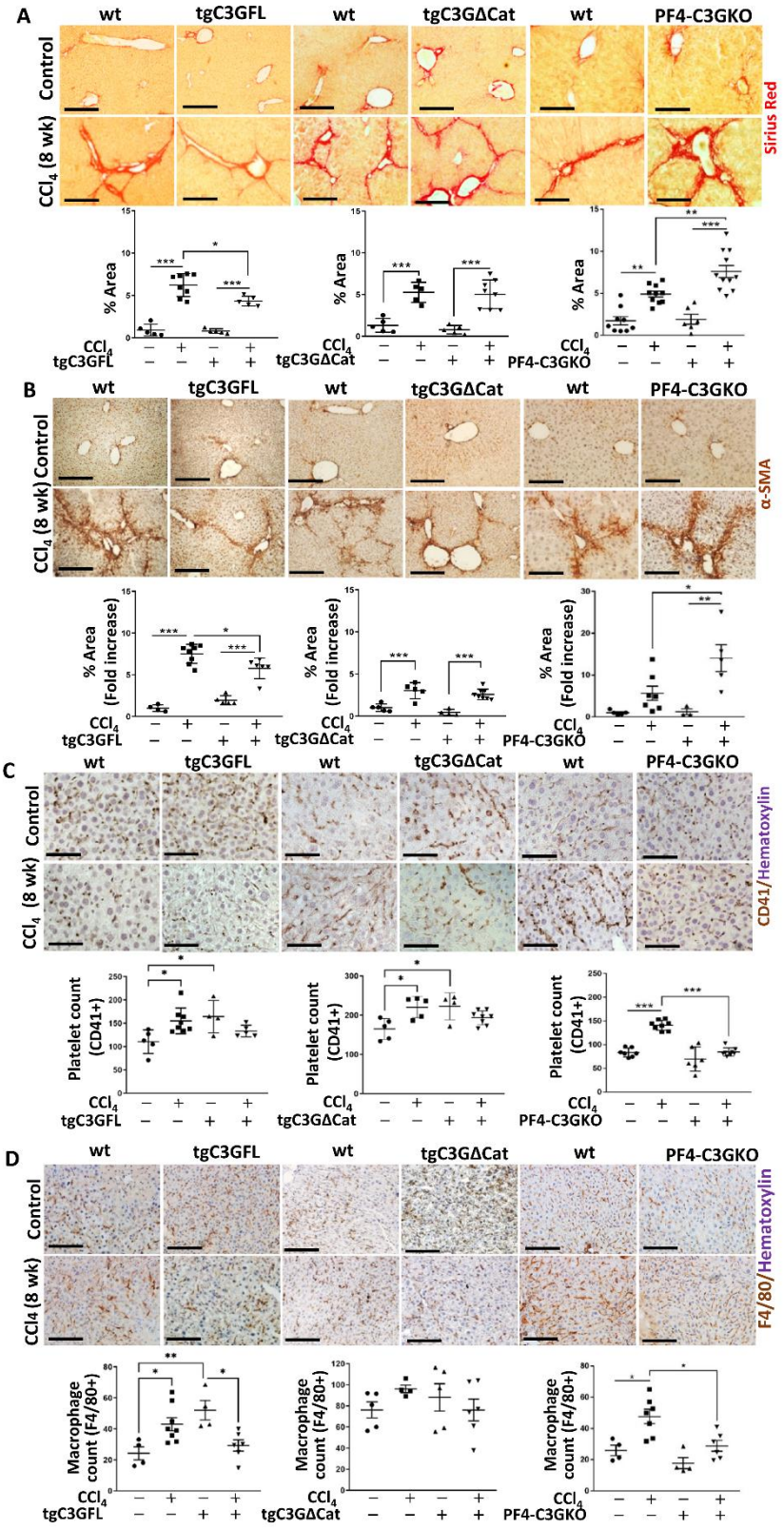
A
wt
tgC3GFL
wt
tgC3GΔCat
wt
PF4-C3GKO
Control
CCl4 (8 wk)
Sirius Red
% Area
CCl4
tgC3GFL
tgC3GΔCat
PF4-C3GKO
B
α-SMA
% Area (Fold increase)
C
CD41/Hematoxylin
Platelet count (CD41+)
D
F4/80/Hematoxylin
Macrophage count (F4/80+)

Figure 2

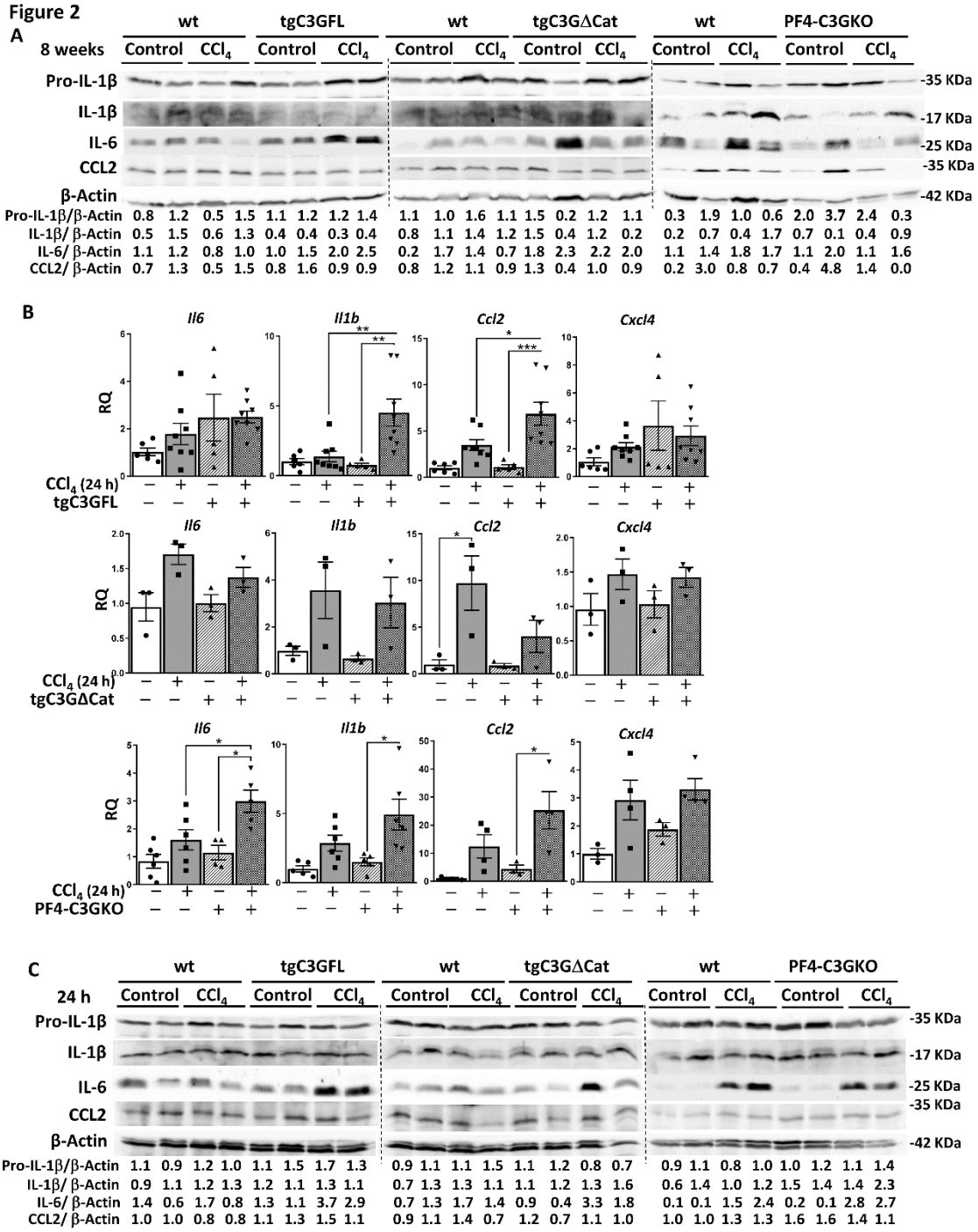
A
8 weeks
wt
tgC3GFL
wt
tgC3GΔCat
wt
PF4-C3GKO
Control
CCl4
Pro-IL-1β
IL-1β
IL-6
CCL2
β-Actin
-35 KDa
-17 KDa
-25 KDa
-35 KDa
-42 KDa
Pro-IL-1β/β-Actin 0.8 1.2 0.5 1.5 1.1 1.2 1.2 1.4 1.1 1.0 1.6 1.1 1.5 0.2 1.2 1.1 0.3 1.9 1.0 0.6 2.0 3.7 2.4 0.3
IL-1β/ β-Actin 0.5 1.5 0.6 1.3 0.4 0.4 0.3 0.4 0.8 1.1 1.4 1.2 1.5 0.4 1.2 0.2 0.2 0.7 0.4 1.7 0.7 0.1 0.4 0.9
IL-6/ β-Actin 1.1 1.2 0.8 1.0 1.0 1.5 2.0 2.5 0.2 1.7 1.4 0.7 1.8 2.3 2.2 2.0 1.1 1.4 1.8 1.7 1.1 2.0 1.1 1.6
CCL2/ β-Actin 0.7 1.3 0.5 1.5 0.8 1.6 0.9 0.9 0.8 1.2 1.1 0.9 1.3 0.4 1.0 0.9 0.2 3.0 0.8 0.7 0.4 4.8 1.4 0.0
B
Il6
Il1b
Ccl2
Cxcl4
RQ
CCl4 (24 h)
tgC3GFL
tgC3GΔCat
PF4-C3GKO
C
24 h
wt
tgC3GFL
wt
tgC3GΔCat
wt
PF4-C3GKO
Control
CCl4
Pro-IL-1β
IL-1β
IL-6
CCL2
β-Actin
-35 KDa
-17 KDa
-25 KDa
-35 KDa
-42 KDa
Pro-IL-1β/β-Actin 1.1 0.9 1.2 1.0 1.1 1.5 1.7 1.3 0.9 1.1 1.1 1.5 1.1 1.2 0.8 0.7 0.9 1.1 0.8 1.0 1.0 1.2 1.1 1.4
IL-1β/ β-Actin 0.9 1.1 1.2 1.3 1.2 1.1 1.3 1.1 0.7 1.3 1.3 1.1 1.1 1.2 1.3 1.6 0.6 1.4 1.0 1.2 1.5 1.4 1.4 2.3
IL-6/ β-Actin 1.4 0.6 1.7 0.8 1.3 1.1 3.7 2.9 0.7 1.3 1.7 1.4 0.9 0.4 3.3 1.8 0.1 0.1 1.5 2.4 0.2 0.1 2.8 2.7
CCL2/ β-Actin 1.0 1.0 0.8 0.8 1.1 1.3 1.5 1.1 0.9 1.1 1.4 0.7 1.2 0.7 1.1 1.0 1.0 1.0 1.3 1.3 1.6 1.6 1.4 1.1

Figure 3

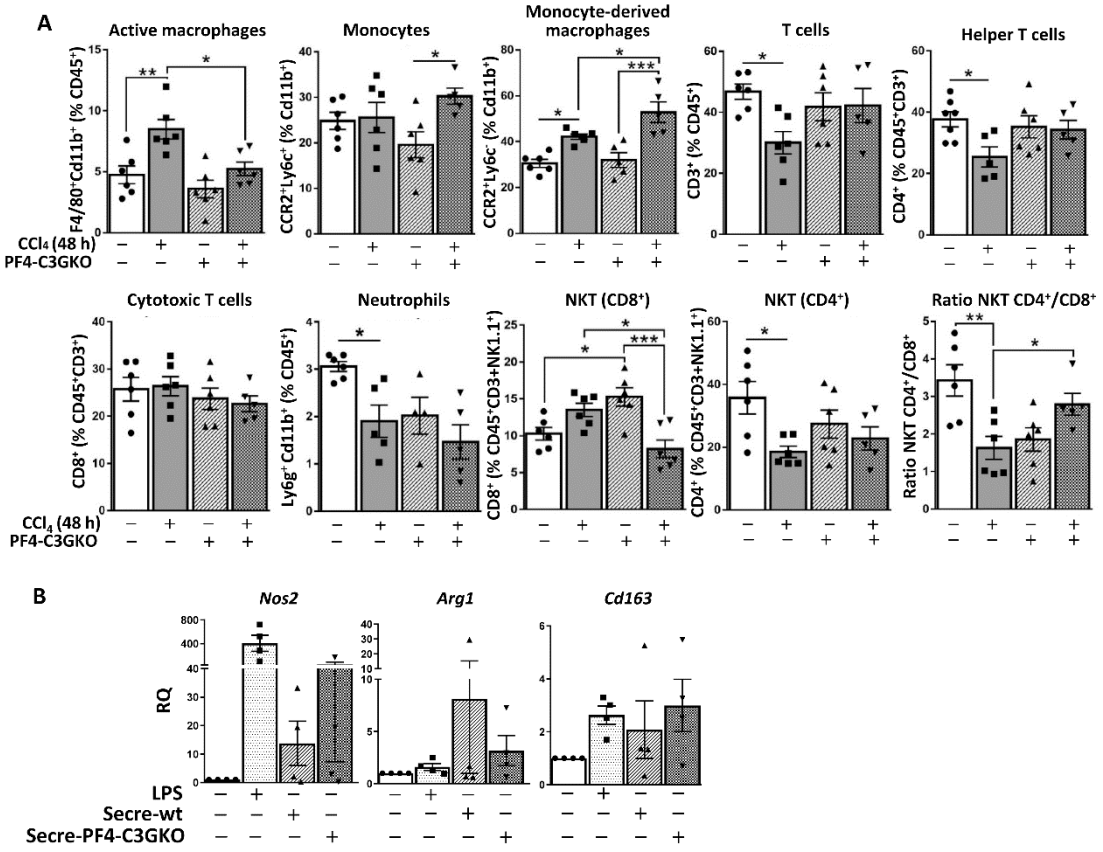
A
Active macrophages
Monocytes
Monocyte-derived macrophages
T cells
Helper T cells
F4/80+Cd11b+ (% CD45+)
CCR2+Ly6c- (% Cd11b+)
CD3+ (% CD45+)
CD4+ (% CD45+CD3+)
CCl4 (48 h)
PF4-C3GKO
Cytotoxic T cells
Neutrophils
NKT (CD8+)
NKT (CD4+)
Ratio NKT CD4+/CD8+
CD8+ (% CD45+CD3+)
Ly6g+ Cd11b+ (% CD45+)
CD8+ (% CD45+CD3+NK1.1+)
CD4+ (% CD45+CD3+NK1.1+)
Ratio NKT CD4+/CD8+
B
Nos2
Arg1
Cd163
RQ
LPS
Secre-wt
Secre-PF4-C3GKO

Figure 4

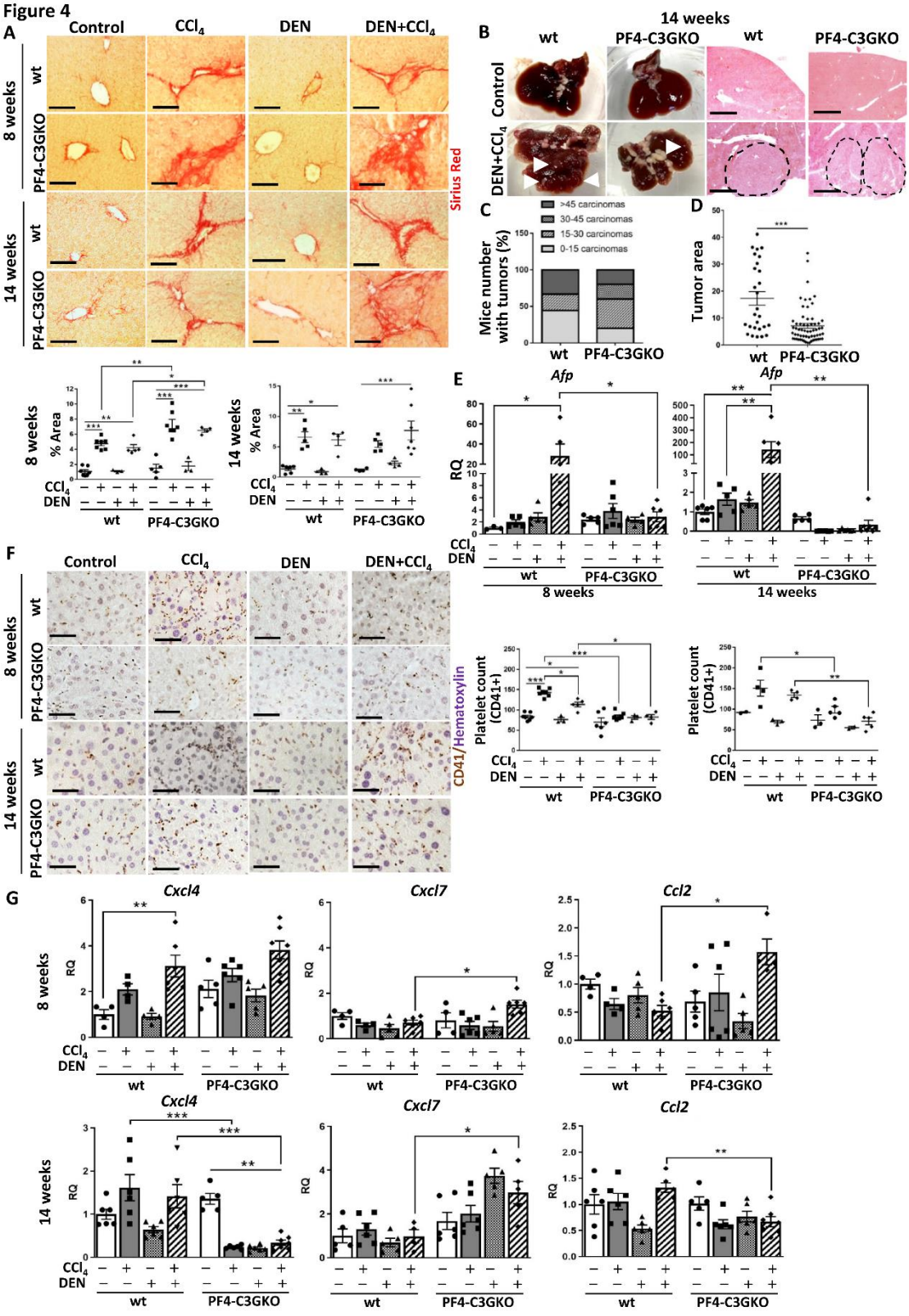
A
Control
CCl4
DEN
DEN+CCl4
8 weeks
14 weeks
wt
PF4-C3GKO
Sirius Red
B
14 weeks
wt
PF4-C3GKO
Control
DEN+CCl4
C
>45 carcinomas
30-45 carcinomas
15-30 carcinomas
0-15 carcinomas
Mice number with tumors (%)
D
Tumor area
8 weeks
% Area
14 weeks
% Area
E
Afp
RQ
8 weeks
14 weeks
F
CD41/Hematoxylin
Platelet count (CD41+)
G
Cxcl4
Cxcl7
Ccl2
RQ
8 weeks
14 weeks

Figure 5

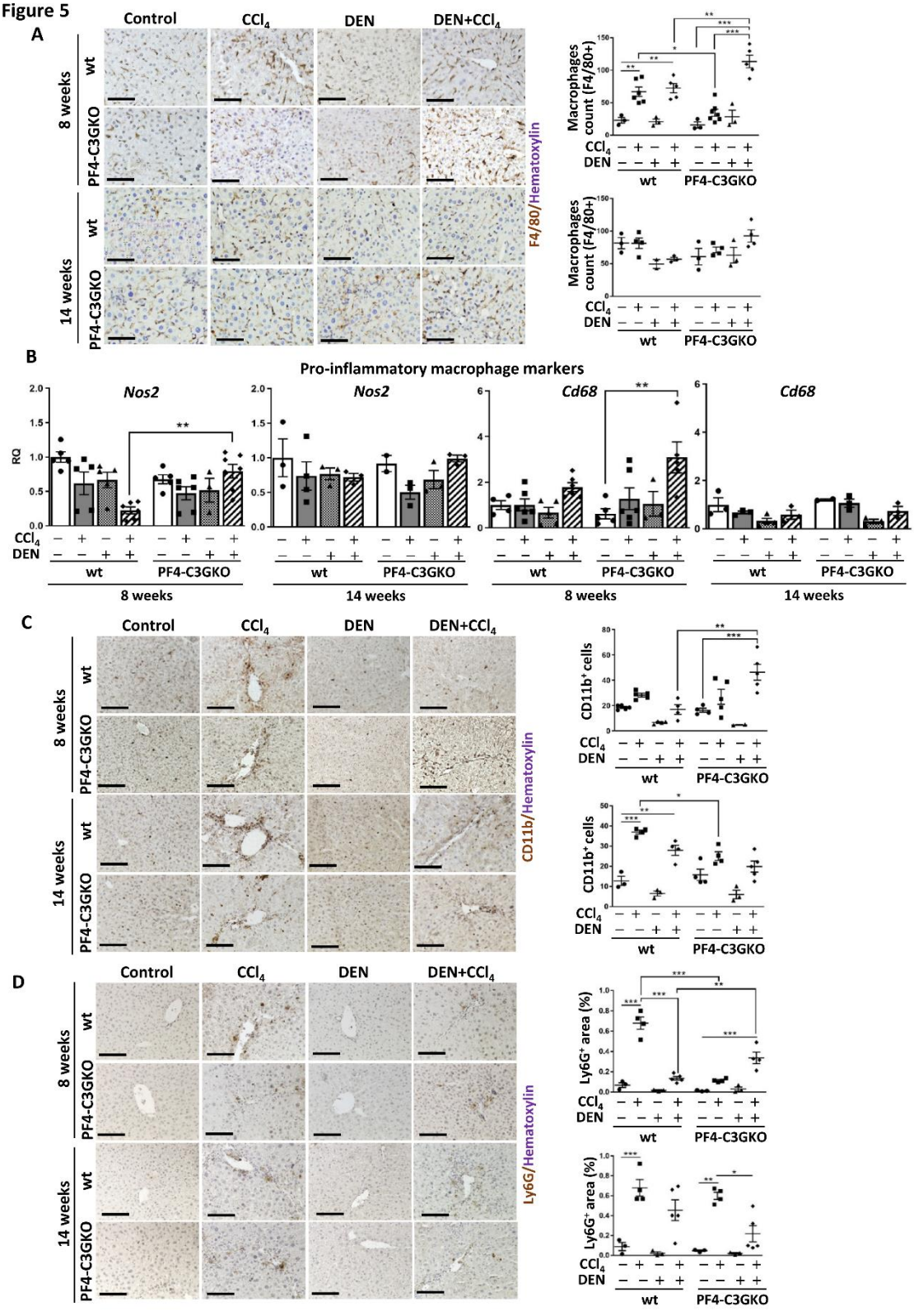
A
Control
CCl4
DEN
DEN+CCl4
8 weeks
14 weeks
wt
PF4-C3GKO
F4/80/Hematoxylin
Macrophages count (F4/80+)
CCl4
DEN
wt
PF4-C3GKO
B
Pro-inflammatory macrophage markers
Nos2
Cd68
RQ
8 weeks
14 weeks
C
CD11b/Hematoxylin
CD11b+ cells
D
Ly6G/Hematoxylin
Ly6G+ area (%)

Figure 6

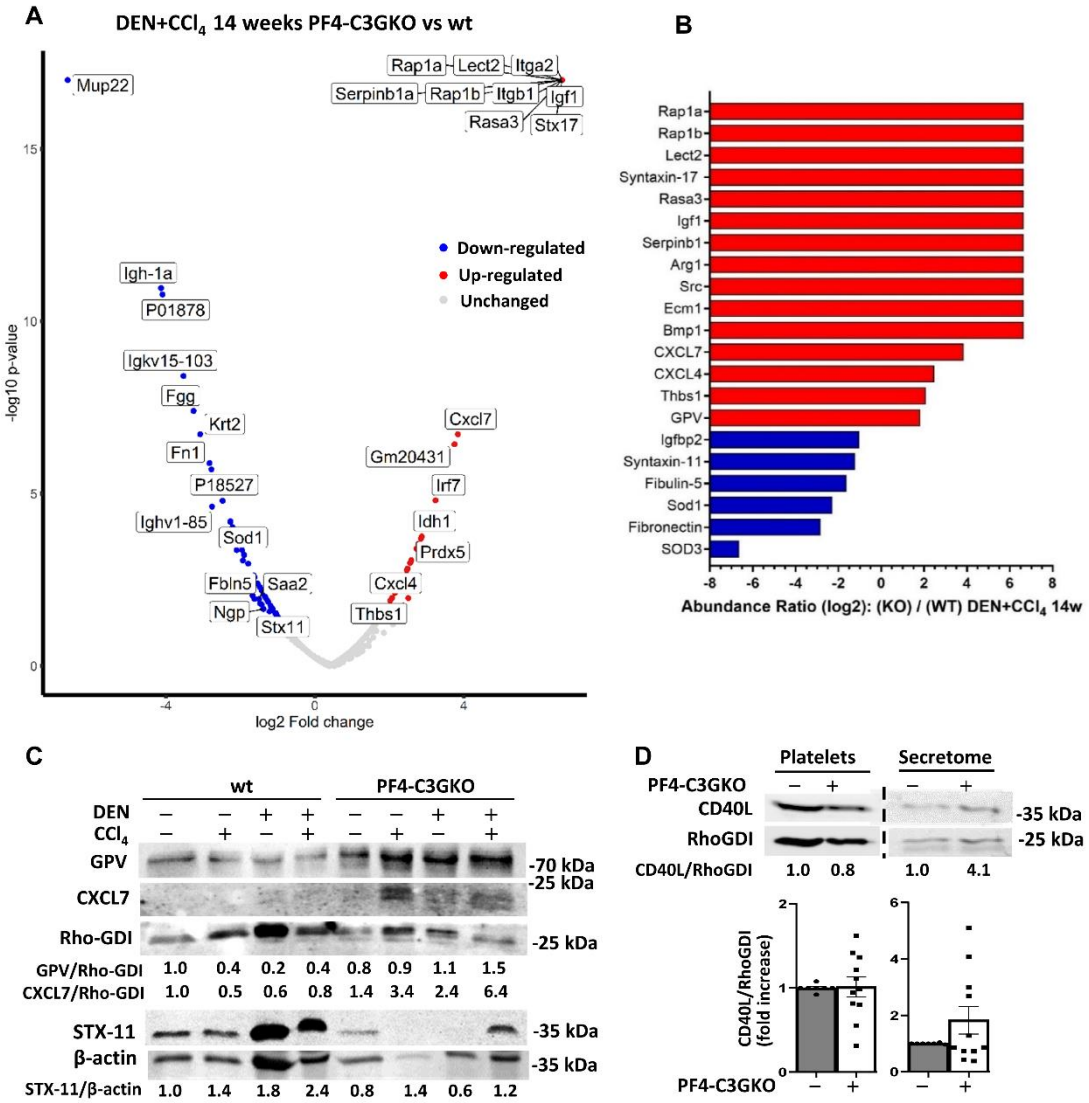
A
DEN+CCl4 14 weeks PF4-C3GKO vs wt
Down-regulated
Up-regulated
Unchanged
-log10 p-value
log2 Fold change
Mup22
Igh-1a
P01878
Igkv15-103
Fgg
Krt2
Fn1
P18527
Ighv1-85
Sod1
Fbln5
Saa2
Ngp
Stx11
Rap1a
Lect2
Itga2
Serpinb1a
Rap1b
Itgb1
Igf1
Rasa3
Stx17
Cxcl7
Gm20431
Irf7
Idh1
Prdx5
Cxcl4
Thbs1
B
Rap1a
Rap1b
Lect2
Syntaxin-17
Rasa3
Igf1
Serpinb1
Arg1
Src
Ecm1
Bmp1
CXCL7
CXCL4
Thbs1
GPV
Igfbp2
Syntaxin-11
Fibulin-5
Sod1
Fibronectin
SOD3
Abundance Ratio (log2): (KO) / (WT) DEN+CCl4 14w
C
wt
PF4-C3GKO
DEN
CCl4
GPV
CXCL7
Rho-GDI
-70 kDa
-25 kDa
-25 kDa
GPV/Rho-GDI 1.0 0.4 0.2 0.4 0.8 0.9 1.1 1.5
CXCL7/Rho-GDI 1.0 0.5 0.6 0.8 1.4 3.4 2.4 6.4
STX-11
β-actin
-35 kDa
-35 kDa
STX-11/β-actin 1.0 1.4 1.8 2.4 0.8 1.4 0.6 1.2
D
Platelets
Secretome
PF4-C3GKO
CD40L
RhoGDI
-35 kDa
-25 kDa
CD40L/RhoGDI 1.0 0.8 1.0 4.1
CD40L/RhoGDI (fold increase)
PF4-C3GKO

Supplementary information

-Supplementary Material and Methods, including table 1

-Supplementary figures 1-13 and tables 2-5

MATERIAL AND METHODS

Genetically modified mice models

Transgenic mice overexpressing human full-length C3G (tgC3GFL (C57BL/6J-Tg(PF4-RAPGEF1)6A6Cgu/Cnbc) or C3G lacking the catalytic domain (tgC3GΔCat (C57BL/6J-Tg(PF4-RAPGEF1*)8A3Cgu/Cnbc)) in megakaryocytes and platelets (under *pf4* promoter) and a conditional megakaryocyte/platelet C3G knockout (Rapgef1flox/flox;*pf4*-Cre (C57BL/6N-Rapgef1tm(flox/flox)Wtsi/J), hereinafter PF4-C3GKO) mouse, previously described and characterized [31–36], were used (males and females). Each transgenic and knockout mouse has a different control, consisting in the corresponding wild-type (wt) littermates (wt-C3GFL, wt-C3GΔCat and PF4-C3G-wt), which may show some differences in their behavior since they have different genetic backgrounds.

Induction of liver fibrosis and HCC associated with fibrosis

To induce liver fibrosis in mice, an established model based on CCl_4 treatment was used [37]. Genetically modified mice and their respective wt (8–10-week-old males and females) controls were treated with 0,48 g/kg CCl_4 (Sigma-Aldrich # 319961; Merck, Darmstadt, Germany) in 10% mineral oil or with the vehicle (controls) twice a week for 4 or 8 weeks by intraperitoneal administration. Short-term treatments of 24-48h were also performed.

HCC associated with fibrosis was induced by treatment with DEN (diethylnitrosamine) (Sigma-Aldrich N0258-1G) and CCl_4 [38]. PF4-C3GKO and wt mice (males and females) were treated with DEN, CCl_4, DEN+CCl_4 or vehicles (mineral oil/PBS) by intraperitoneal injection. DEN (10mg/Kg) in PBS or PBS was administered to 14-day old mice. Four weeks later, CCl_4 (0,48 g/kg) treatment was initiated, being maintained for 8 or 14 weeks.

Analysis of fibrosis in liver sections by Sirius Red staining

Dewaxed liver paraffin sections were incubated with a 0.1% Picro-Sirius Red (Direct Red 80 (Sigma-Aldrich 365548) solution saturated with picric acid (Sigma-Aldrich P6744-1GA) for 1h to stain collagen fibers. Then, they were washed with 0.5% (vol:vol) acetic acid: water. After dehydration, sections were mounted using DPX and images were taken using an Eclipse TE300, Nikon microscope coupled to a Nikon Digital Sight DS-U2 camera (20X) (Nikon, Melville, New Jersey, USA).

Liver tissue paraffin embedding and hematoxylin/eosin staining

Liver samples fixed in 4% PFA (paraformaldehyde) o/n were embedding in paraffin as previously described [30]. Essentially, samples were washed in cold PBS and dehydrated by incubation in increasing concentrations of ethanol, and xylene. Then, samples were embedded in paraffin wax. Sections (5-7 µm) were generated with the microtome and mounted into APES pre-coated slides.

To perform hematoxylin/eosin staining liver paraffin sections were dewaxed by incubation in decreasing concentrations of ethanol. Then, sections were incubated with

hematoxylin (Panreac 255298.1610; Merck, Darmstadt, Germany) (17 min), washed with water, incubated with eosin 1% (Panreac 251301.1611) (9 min) and washed with water. After dehydration, they were mounted using DPX (Dibutylphthalate Polystyrene Xylene (VWR Chemicals 1.00579.0500; Radnor, Pennsylvania, USA). Images were taken using a Leica DMC 4500 phase-contrast microscope (Leica, Wetzlar, Germany).

Immunohistochemistry analysis in liver sections

After deparaffinization and rehydration, antigen retrieval with citrate buffer (10 mM, pH=6) was performed [23]. Dewaxed liver paraffin sections were transferred to a 10 mM citrate solution (pH 6) and heated for 20 min to uncover antigens. After cooling down, sections were treated in the following way for immunohistochemistry (IH): ethanol 90% (3 min); ethanol 100% (3 min); 3% H_2O_2 in methanol 100% (20 min); ethanol 100% (3 min); ethanol 90% (3 min) to block endogenous peroxidase and washed with H_2O (5 min) and PBS (5 min). Next, slides were permeabilized with 0,5% Triton X-100-PBS (5 min), washed with PBS (5 min) and incubated in blocking buffer (3% BSA-1,5% normal goat serum-PBS (Invitrogen Thermo-Fisher, PCN5000; Waltham, Massachusetts, USA) 30 min at RT, washed with PBS and incubated with the following primary antibodies against: α-SMA (Dako M0851; 1:50, Santa Clara, California, USA), F4/80 (Bio-Rad MCA497; 1:2; Hercules, California, USA), CD41 (Abcam ab181582; clone EPR17876; 1:50; Cambridge, UK), CD11b (Novus-NB110-89474SS; polyclonal; 1:100; Cambridge, UK) and Ly6G (R&D MAB1037; clone RB6-8C5; 1:50; Minneapolis, Minnesota, USA) in blocking buffer overnight at 4ºC (in a wet chamber). After washing with PBS, sections were incubated with the corresponding biotinylated secondary antibody for 1h at RT. Then, they were washed with PBS, incubated with avidin/biotin (1:1; Vector Laboratories PK-6100; Newark, California, USA) for 30 min at RT in dark, washed with PBS and revealed with DAB (3,3′-diaminobenzidine, Vector Laboratories, SK-41000). Then, they were washed with H_2O, incubated with hematoxylin (1 min) and washed with H_2O. Sections were then dehydrated and mounted using DPX.

Images (15-20/sample) were taken using an Eclipse TE300, Nikon microscope coupled to a Nikon Digital Sight DS-U2 camera (20X) or a Leica DMC 4500 microscope.

Analysis of non-parenchymal liver cells by flow cytometry

Isolated NPCs were incubated with the following antibodies: Rat Anti-Mouse CD45-FITC, clone I3/2.3 (1/200) (SouthernBiotech; Birmingham, Alabama, USA), PE-Cy™7 Rat Anti-Mouse Ly-6G, clone 1A8 (1/100) (BD Pharmingen; Franklin Lakes, New Jersey, USA); APC F4/80 Monoclonal Antibody, clone BM8 (1:25) (eBioscience; San Diego, California, USA); PE/Cyanine7 anti-mouse/human CD11b Antibody, clone M1/70 (BioLegend; San Diego, California, USA); PE/Cyanine7 anti-mouse CD3, clone 145-2C11 (1/100) (BioLegend); APC Anti-Mouse NK-1.1, clone PK136 (1/25), (BD Pharmigen); PE Rat Anti-Mouse CD8a, clone 53-6.7 (1/50) (BD Pharmingen); PerCP/Cyanine5.5 Anti-mouse CD4, clone GK1.5 (1/100) (BioLegend); FITC anti-mouse Ly-6C, clone HK1.4 (1/100) (BioLegend); and PE anti-mouse CD192 (CCR2) (1/200) (BioLegend A) or their corresponding isotype controls for 20 min at RT in the dark. After washing with PBS, NPCs were resuspended in PBS. Flow cytometry analysis was performed in a FACSCanto II and data were analyzed using Cytomics FC500 with CXP program. The results were referred to the % of CD45 positive cells, according to each combination.

Preparation of platelet-rich plasma, platelet stimulation with ADP and secretome generation

Blood collected from the heart was placed in EDTA-pretreated tubes. It was centrifuged at 100g 10 min, and the supernatant and interphase were centrifuged at 100g 5 min to eliminate erythrocytes (pellet), while keeping the supernatant corresponding to platelet-rich plasma (PRP).

PRPs were centrifuged at 1300g 5 min at RT. Platelets were resuspended in Tyrode's Hepes buffer and allowed to rest at RT for 30 min. Then, platelets (2-3x10^7) were stimulated with 10μM ADP for 15 min in PBS-containing 2 mM $CaCl_2$ at 37ºC and centrifuged at 2500g, getting the supernatant with the secretome.

RNA isolation and RT-qPCR

Total RNA isolation and RT-qPCR analysis was performed as previously described [29]. Briefly, total RNA was isolated using NucleoSpin RNA kit (Macherey-Nagel 740955.50; Dueren, Germany) and reverse transcribed using SuperScript IV-RT kit (Invitrogen Thermo-Fisher 18090200) and reverse transcribed using SuperScript III-RT kit (Invitrogen Thermo-Fisher 12574026). cDNA was amplified using the following specific primers for *Afp, Ccl2, Cxcl4, Cxcl7, Cd68, Cd163, Hgf, Il6, Il1b, Nos2, Tgfb1* and *Gusb* to normalize (Table 1). Ct (threshold cycle) for a gene minus Ct for *Gusb*=ΔCt was calculated and then, referred to non-silenced control values (sample ΔCt-non-silenced ΔCt= ΔΔCt) to calculate RQ ($2^{-\Delta\Delta Ct}$).

Supplementary table 1-Sequences of primers used for RT-qPCR analysis. Primers´sequences for *Afp, Ccl2, Cxcl4, Cxcl7, Cd68, Cd163, Hgf, Il6, Il1b, Nos2, Tgfb1* and *Gusb are listed.*

mRNA	Forward primer (5´→3´)	Reverse primer (5´→3´)
Afp	TGTTGCCAAGGAAACTCG	GCAGCACTCTGCTATTTTGC
Ccl2	CTGCTGCTACTCATTCACCA	CCATTCCTTCTTGGGGTCAG
Cxcl4	CCACCCTGAAGAATGGGAGG	GGCAGCTGATACCTAACTCTCC
Cxcl7	CAACGGAAATCGCCTCCAGT	AATGTTGCAGAGGTTGCTTGG
Cd68	CTAGGACCGCTTATAGCCCAA	GATGGCAGGAGAGTAACGGC
Cd163	GTGCTGGATCTCCTGGTTGTAA	AGGAGCGTTAGTGACAGCAG
Hgf	TGACCTGCAACGGTGAAAGC	TGTGGGGTACTGCGAATCC
Il6	TGCCTTCTTGGGACTGATGC	TGAAGTCTCCTCTCCGGACT
Il1b	ATCTCGCAGCAGCACATCAA	ACGGGAAAGACACAGGTAGC
Nos2	GGTGAAGGGACTGAGCTGTT	ACGTTCTCCGTTCTCTTGCAG
Tgfb1	ATGAACCGGCCCTTCCTGCT	TTGGTATCCAGGGCTCTCCGGT
Gusb	AAAATGGAGTGCGTGTTGGGTCG	CCACAGTCCGTCCAGCGCCTT

Western-blot analysis

Western-blot analysis was carried out as previously described [29]. Membranes were probed with primary antibodies against CCL2 (Biocompare-Boster A00056-4; polyclonal, dilution 1:1000; Pleasanton, California USA), IL-6 (Santa Cruz Biotechnology sc-57315; clone 10E5; dilution 1:500; Dallas, Texas, USA), IL-1β (Proteintech 16806-1-AP; polyclonal; dilution 1:1000; Rosemont, Illinois, USA), GPV (BD Pharmingen 552992; clone 1C2; 1:1000), CXCL7 (R&D systems MAB10911; clone 159703; 1:500), Syntaxin 11 (Synaptic System 110113; polyclonal; 1:1000; Goettingen, Germany), CD40L (Abcam 52750; clone EP462E; 1:500; Cambridge, UK) , Rho-GDI (Santa Cruz Biotechnology sc-373724; clone G-2;1:1000) and β-Actin (Cell Signaling Technology CST 3700, clone 8H10D10; 1:2500; Danvers, Massachusetts, USA) to normalize.

Analysis of platelet releasate in thrombin-stimulated platelets

Platelets (1×10^9) were stimulated with thrombin (0.2 U/ml) and the secretome purified as described [36]. The levels of HGF, IL-1α, PF4 and CCL2 in the releasate of PF4-C3GKO and tgC3GFL platelets were quantified using the Proteome Profiler Mouse Angiogenesis Array Kit (R&D Systems ARY015), following the manufacturer´s instructions.

Analysis of serum AST and ALT activities

AST (aspartate amino transferase) activity was measured using L-aspartate as substrate, leading to oxalacetate, which is converted into malate by adding malate dehydrogenase and NADPH (that generates NAD+). ALT (alanine aminotransferase) activity was measured in the same way using L-alanine as substrate, and lactate dehydrogenase and NADH were added to generate lactate and NAD+. The decrease in NADH absorbance (at 340 nm) per min is used to calculate these activities (Spinreact 150014 (AST) and 150025 (ALT); Spinreact, Barcelona, Spain).

Isolation of peritoneal macrophages and stimulation

Mice were treated with 3% thioglycolate (BD 225650) by intraperitoneal injection and macrophages were isolated 4 days later. Then, PBS was injected into the peritoneal cavity and after 10-15 seconds the peritoneum fluid was aspirated with a syringe. Cells in the fluid were recovered by centrifugation (6 min at 1200 rpm and at 4ºC) and erythrocytes lysed. Afterwards, cells resuspended in DMEM supplemented with 10% FBS were seeded and maintained in culture for 2h. Non-attached cells were removed while keeping macrophages in 10% FBS DMEM for 24h. Then, the medium was replaced by a new one supplemented with 2%FBS and 24h after, macrophages were stimulated with LPS (lipopolysaccharide) (50ng/mL) or platelet secretomes for 24h.

Wide proteomic analysis

PRPs from PF4-C3GKO and wt mice treated with DEN+CCl4 or the vehicle for 14 weeks were used. PRPs´ protein extracts digested with trypsin and peptides were analyzed by liquid nano chromatography (nano Easy-nLC 1000, Thermo Scientific, Walthan, Massachusetts, USA) coupled to a high-resolution mass spectrometer Q-Exactive HF (Thermo Scientific) at UCM proteomic center. MS/MS data were acquired in the data-dependent acquisition (DDA) mode of the MS. MS scans were acquired at m/z range of 350 to 1800 Da followed by data-dependent MS/MS scan (with threshold of 0.01) of the 15 most abundance precursors with charges of 2-5 in MS scans for high-energy collision dissociation (HCD) fragmentation with a dynamic exclusion of 10 s and normalized collision energy (NC) of 20. Peptide spectrum matches were filtered to a false discovery rate (FDR) of > 1%. MS/MS spectra corresponding to the different samples were analyzed using Proteome Discoverer 2.4 (Thermo Scientific,) software with MASCOT v.2.6.1. search engine and Uniprot databases for Mus musculus (55432 sequences). Search parameters included carbamidomethylation of cysteines as fixed modification, oxidation of methionine and N-terminal acetylation as variable modifications, trypsin as enzyme and a maximum of 2 missed cleavages allowed. The precursor mass tolerance was 10 ppm and the fragment mass tolerance was 0.02 Da. The validation was based on q-value from Percolator algorithm, with FDR > 0.01.

Statistical analysis by t test was performed. Significant changes in the abundance of proteins between PF4-C3GKO and wt mice treated with DEN+CCl4 PRPs were considered when the P value was <0.05 and the log2 fold change was more than 1.7 or less than -0.7 and statistical changes in the abundance of proteins between PF4-C3GKO

and wt mice were considered when the P value was <0.05 and the log2 fold change was more than 1 or less than -0.9.

Data were subjected to GOGO (Gene ontology) enrichment analyses were carried out using gprofiler2 R package in RStudio v4.2.3 [41]. Proteins that exhibited statistically significant changes (p≤0.05) were classified as over or under-represented. Additionally, enrichment analyses using DAVID (Database for Annotation, Visualization and Integrated Discovery) and Panther software were performed to analyze GOBP (Gene Ontology Biological processes) and KEGG Pathway interactions.

Statistical analysis

Data are represented as the mean ± S.E.M. (n=3-8 mice). Unpaired Student's t-test was used for comparison of two experimental groups and One-way ANOVA or two-way ANOVA for comparing more than two groups with one or two variables, respectively, followed by Tukey or Bonferroni multiple comparison test following statistical software recommendations. Differences were considered significant when p value was p≤0,05 (*); p≤0,01 (**); p≤0,001 (***). GraphPad Prism version 7 was used for the analysis.

Supplementary table 2-Analysis of fibrosis using metavir score system. Mice from the indicated phenotypes were treated with CCl_4 for 8 weeks or with mineral oil (controls) and the degree of fibrosis was analyzed using metavir score system (n=4-8).

Genotype	Treatment (8 weeks)	Metavir score
wt	Control	F0-F1
	CCl_4	F2-F3
tgC3GFL	Control	F0-F1
	CCl_4	F2
wt	Control	F1
	CCl_4	F2-F3
tgC3GΔCat	Control	F0-F1
	CCl_4	F2-F3
wt	Control	F0-F1
	CCl_4	F2
PF4-C3GKO	Control	F1
	CCl_4	F3

(F0: no fibrosis; F1: portal fibrosis; F2: fibrosis in most portal zones and occasional bridging; F3: fibrosis in most portal zones, marked bridging and occasional modules; F4: cirrhosis).

Supplementary table 3-Analysis of fibrosis using metavir score system. Mice from the indicated phenotypes were treated with CCl_4, DEN or DEN+CCl_4 for 8 or 14 weeks or with mineral oil and PBS (controls) and the degree of fibrosis was analyzed using metavir score system (n=4-8).

Genotype	Treatment (8 weeks)	Metavir score	Treatment (14 weeks)	Metavir score
wt	Control	F0-F1	Control	F1
	CCl_4	F2	CCl_4	F3
	DEN	F0-F1	DEN	F1
	DEN+CCl_4	F2-F3	DEN+CCl_4	F3
PF4-C3GKO	Control	F1	Control	F1
	CCl_4	F3	CCl_4	F3
	DEN	F0-F1	DEN	F1
	DEN+CCl_4	F3	DEN+CCl_4	F3-F4

(F0: no fibrosis; F1: portal fibrosis; F2: fibrosis in most portal zones and occasional bridging; F3: fibrosis in most portal zones, marked bridging and occasional modules; F4: cirrhosis).

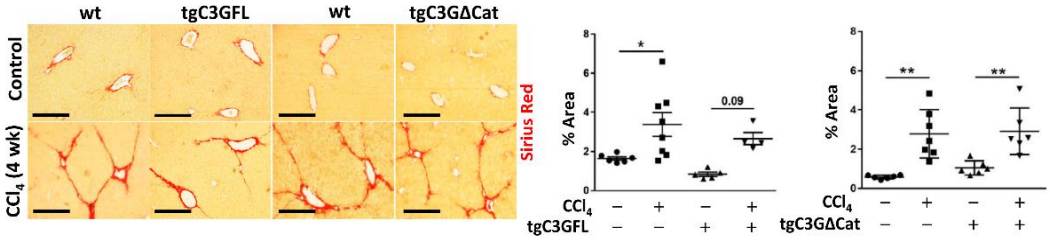

Supplementary figure 1-Effect of C3G overexpression in platelets on CCl_4-induced liver fibrosis. Transgenic mice overexpressing full length C3G (tgC3GFL) or C3G lacking the catalytic domain (tgC3GΔCat) in megakaryocytes and platelets and their corresponding wt counterparts were treated with CCl_4 or vehicle for 4 weeks. A) Analysis of collagen accumulation by Sirius Red staining in liver sections. Left panels, representative microscope images; and right panels, graphics showing quantification of positive areas for each sample and the mean values ± S.E.M. *p≤0,05 and **p≤0,01 compared as indicated (n=3-6). Scale bars: 20 μm.

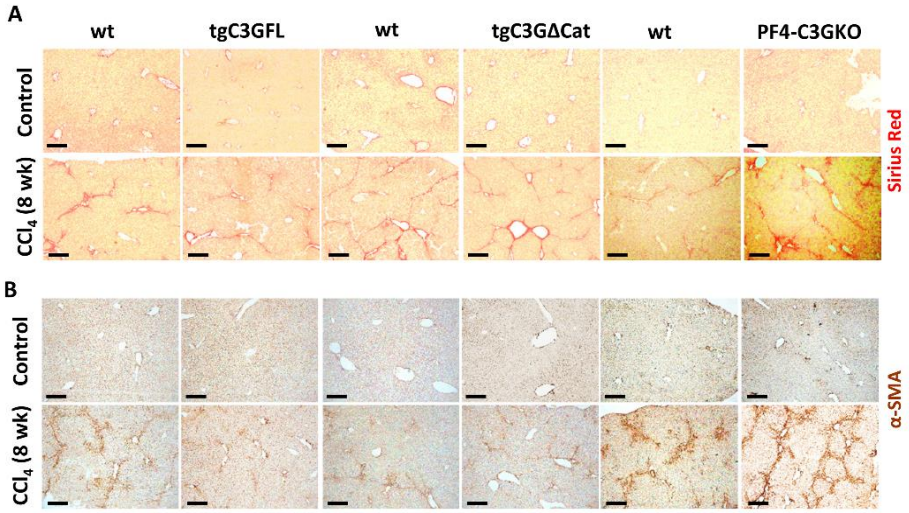

Supplementary figure 2-Low magnification images of collagen and α-SMA accumulation in the liver. Mice overexpressing full length C3G (tgC3GFL) or C3G lacking the catalytic domain (tgC3GΔCat), and those lacking C3G (PF4-C3GKO) in megakaryocytes and platelets and their corresponding wt counterparts were treated with CCl_4 or the vehicle (controls) for 8 weeks. A) Analysis of collagen accumulation by Sirius Red staining in liver sections. B) Analysis of α-SMA levels in liver sections. Images were obtained using a 5x microscope objective. Scale bars: 250 μm.

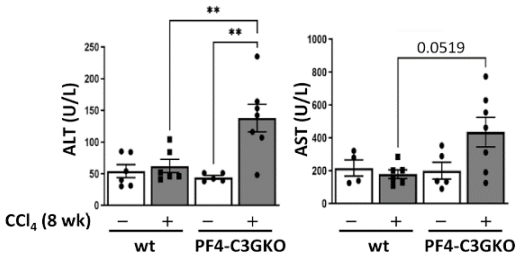

Supplementary figure 3-C3G deficiency in platelets increases liver damage after chronic treatment with CCl_4. Analysis of serum AST and ALT activities in mice lacking C3G (PF4-C3GKO), in megakaryocytes and platelets, and their corresponding wt counterparts, treated with CCl_4 or the vehicle (controls) for 8 weeks.

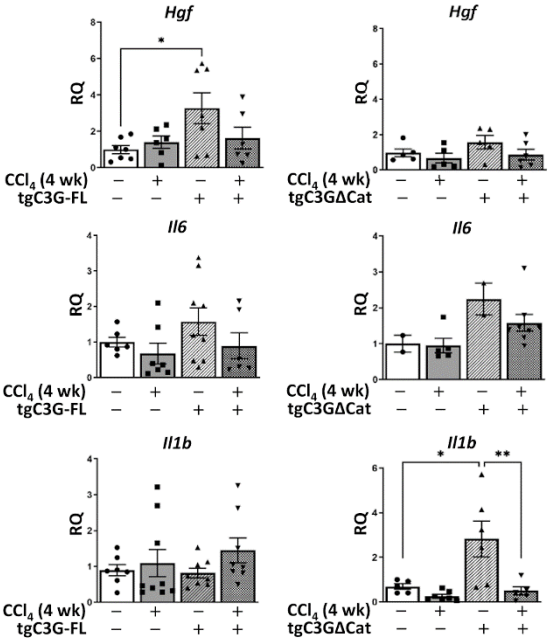

Supplementary figure 4-Regulation by platelet C3G of regulatory factors of fibrosis and inflammation. Transgenic mice overexpressing full length C3G (tgC3GFL) or C3G lacking the catalytic domain (tgC3GΔCat) in megakaryocytes and platelets and their corresponding wt counterparts were treated with CCl_4 or vehicle for 4 weeks. RT-qPCR analysis of *Hgf*, *Il6* and *Il1b* mRNA levels in liver samples. Histograms showing RQ mean values ± S.E.M. *p≤0,05 and **p≤0,01 compared as indicated (n=3-6).

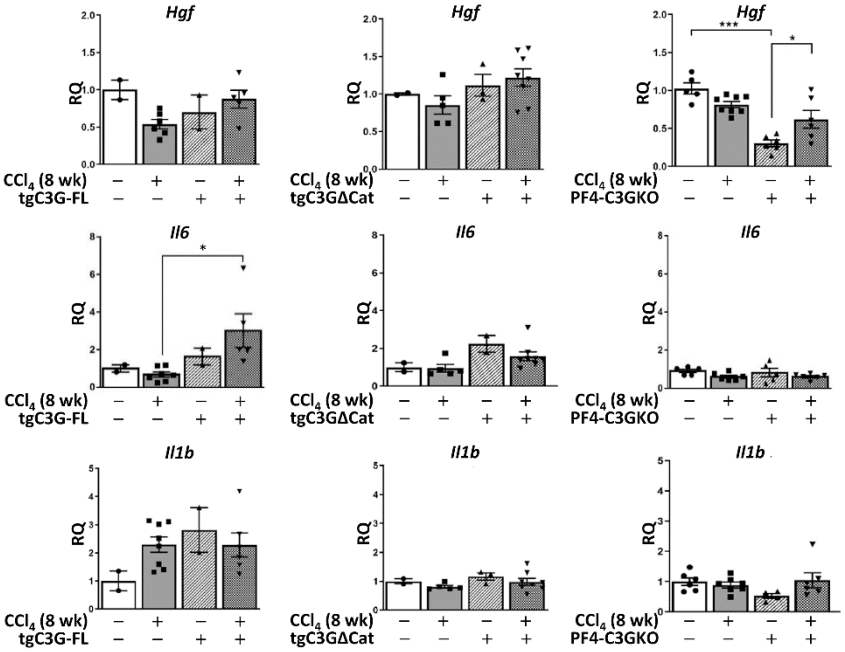

Supplementary figure 5-Regulation of regulatory factors of fibrosis and inflammation by platelet C3G. Mice overexpressing full length C3G (tgC3GFL) or C3G lacking the catalytic domain (tgC3GΔCat), and those lacking C3G (PF4-C3GKO) in megakaryocytes and platelets and their corresponding wt counterparts were treated with CCl_4 or the vehicle (controls) for 8 weeks. RT-qPCR analysis of *Hgf*, *Il6* and *Il1b* mRNA levels in liver samples. Histograms showing RQ mean values ± S.E.M. *p≤0,05 and ***p≤0,001 compared as indicated (n=3-6).

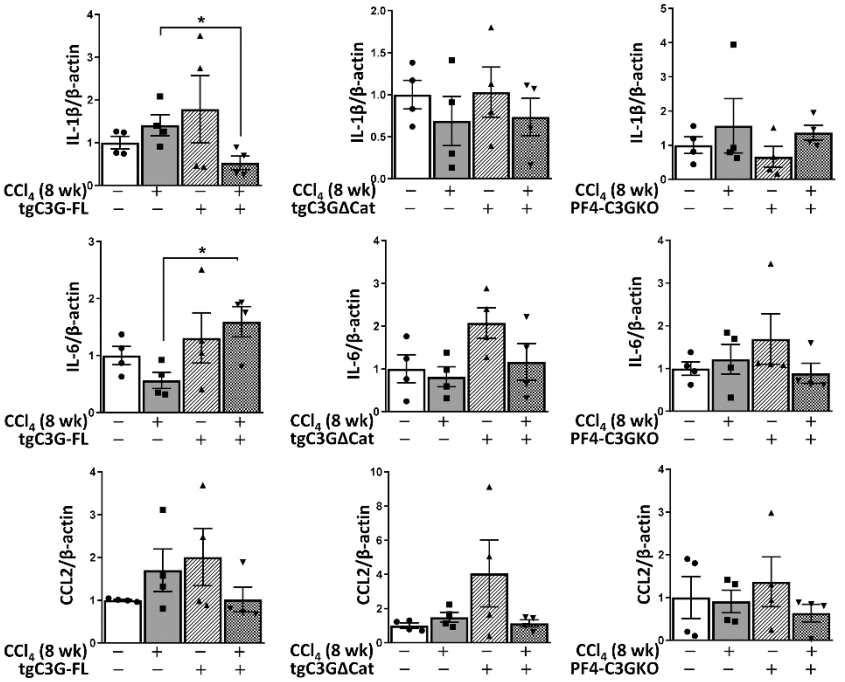

Supplementary figure 6-Quantifications of liver IL-6, IL-1β and CCL2 protein levels. Mice overexpressing full length C3G (tgC3GFL) or C3G lacking the catalytic domain

(tgC3GΔCat), and those lacking C3G (PF4-C3GKO) in megakaryocytes and platelets and their corresponding wt counterparts were treated with CCl_4 or the vehicle (controls) for 8 weeks. IL-6, IL-1β and CCL2 levels were analyzed in liver protein extracts by western-blot. Histograms show mean values ± S.E.M. of the data derived from the densitometric analysis of IL-6, IL-1β and CCL2 normalized with β-Actin. *p≤0,05 compared as indicated (n=3-4).

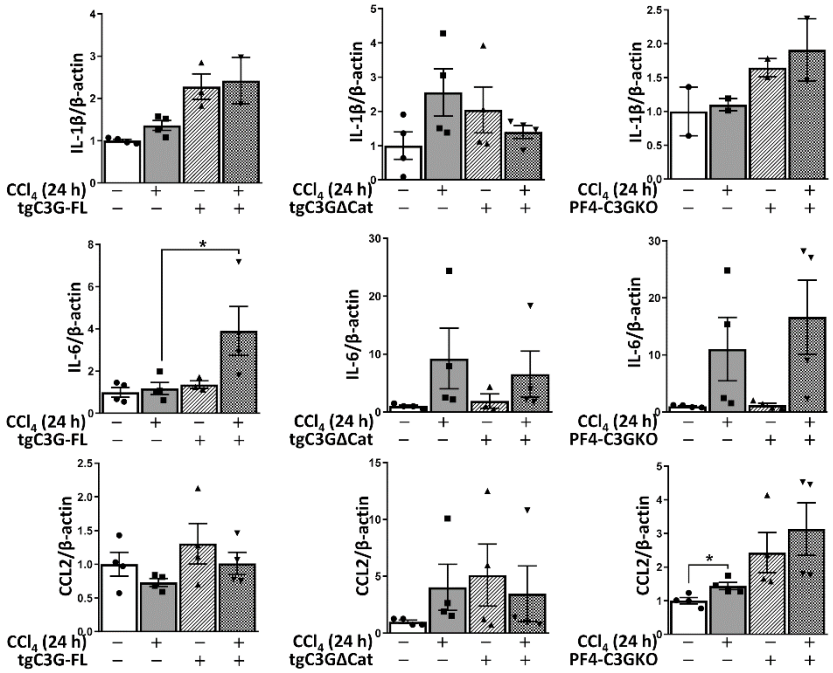

Supplementary figure 7-Quantifications of liver IL-6, IL-1β and CCL2 protein levels. Mice overexpressing full length C3G (tgC3GFL) or C3G lacking the catalytic domain (tgC3GΔCat), and those lacking C3G (PF4-C3GKO) in megakaryocytes and platelets and their corresponding wt counterparts were treated with CCl_4 or the vehicle (controls) for 24h. IL-6, IL-1β and CCL2 levels were analyzed in liver protein extracts by western-blot. Histograms showing mean values ± S.E.M. of the data derived from the densitometric analysis of IL-6, IL-1β and CCL2 normalized with β-Actin. *p≤0,05 compared as indicated (n=3-4).

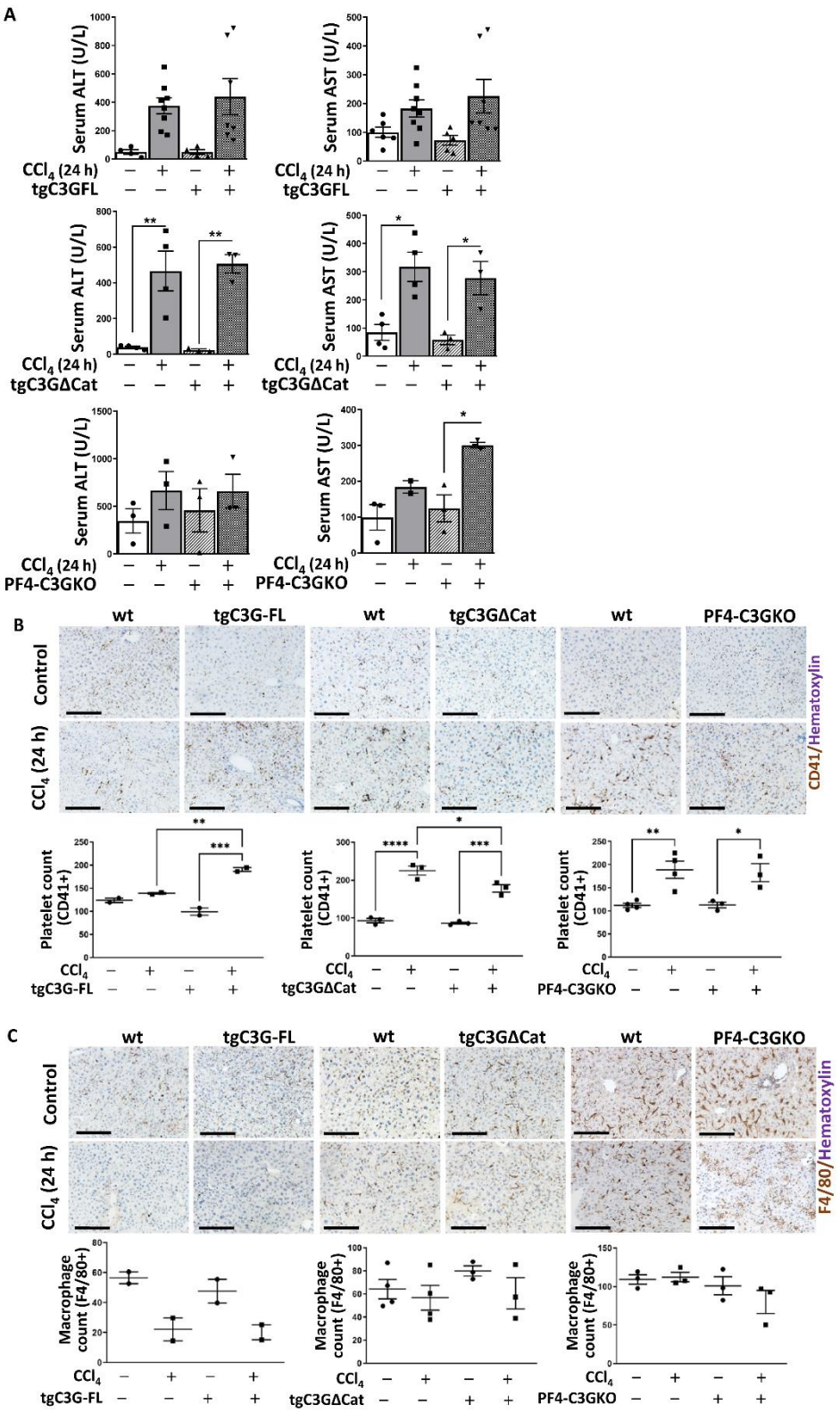

Supplementary figure 8-Effect of platelet C3G on acute liver damage. Mice overexpressing full length C3G (tgC3GFL) or C3G lacking the catalytic domain (tgC3G∆Cat), and those lacking C3G (PF4-C3GKO) in megakaryocytes and platelets and their corresponding wt counterparts were treated with CCl_4 or the vehicle (controls) for 24h. A) Analysis of serum AST and ALT activities. *p≤0,05 and **p≤0,01 compared as indicated (n=3-6). B) Immunohistochemical analysis of liver platelets detected with CD41 antibody. Upper panels, representative microscope images; and lower panels, graphics

showing the number of CD41 positive cells/field for each condition and the mean values ± S.E.M. C) Immunohistochemical analysis of liver macrophages detected with F4/80 antibody. Upper panels, representative microscope images; and lower panels, graphics showing the number of F4/80 positive cells/field for each condition and the mean values ± S.E.M. *p≤0,05, **p≤0,01, ***p≤0,001 and ****p≤0,0001 compared as indicated (n=2-4). Scale bars: 20 μm.

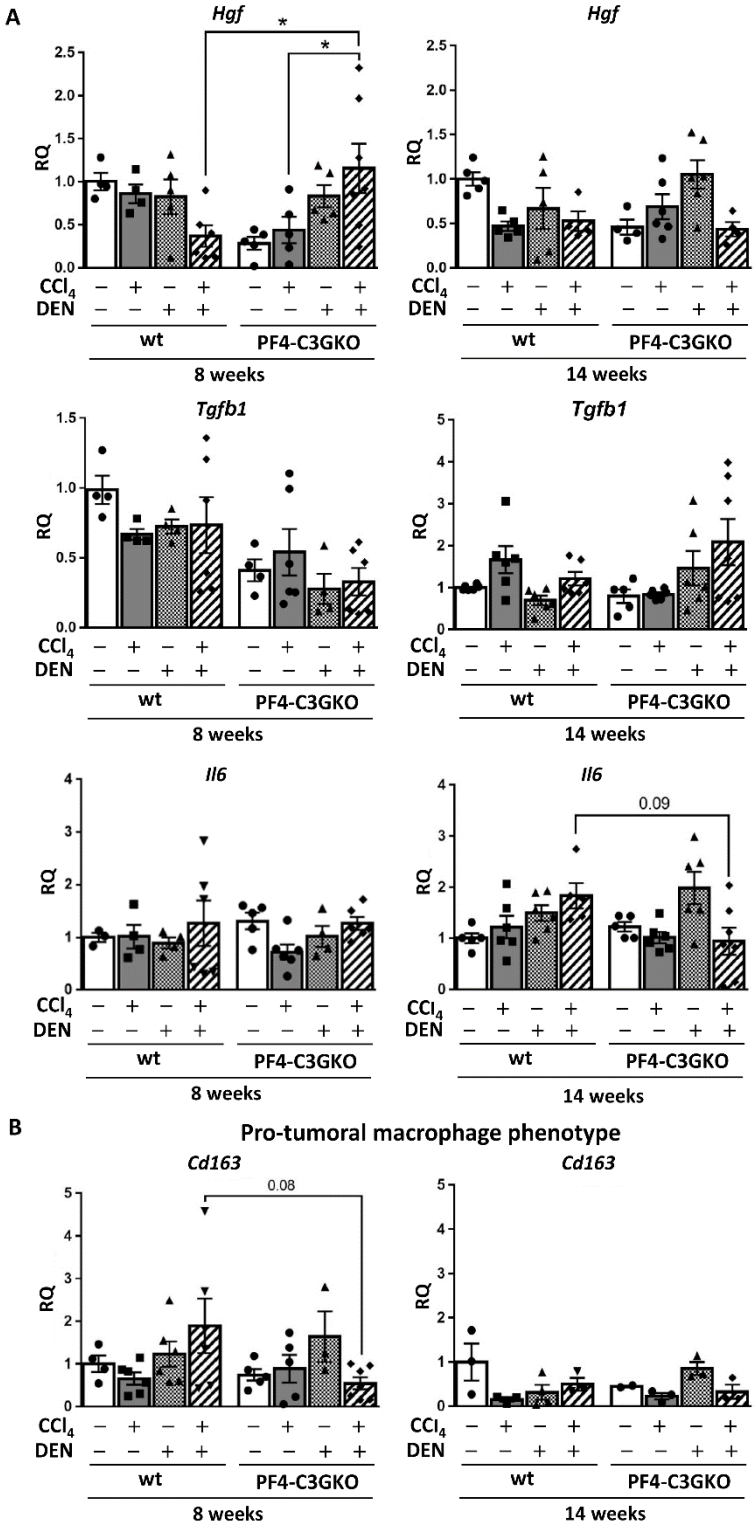

Supplementary figure 9-Impact of C3G deletion in platelets on regulatory factors of fibrosis and inflammation during chemically-induced HCC associated with fibrosis. Mice lacking C3G in megakaryocytes and platelets (PF4-C3GKO) and their corresponding wt counterparts were treated with CCl_4, DEN, DEN+CCl_4 or vehicle for 8 or 14 weeks as indicated. A) RT-qPCR analysis of *Hgf*, *Tgfb1* and *Il6* mRNA levels in liver samples. Histograms showing RQ (individual and mean values ± S.E.M.). B) RT-qPCR analysis of the pro-tumoral macrophage marker *Cd163* mRNA levels in liver samples. Histograms showing RQ (individual and mean values ± S.E.M.). *p≤0,05, compared as indicated (n=4-6).

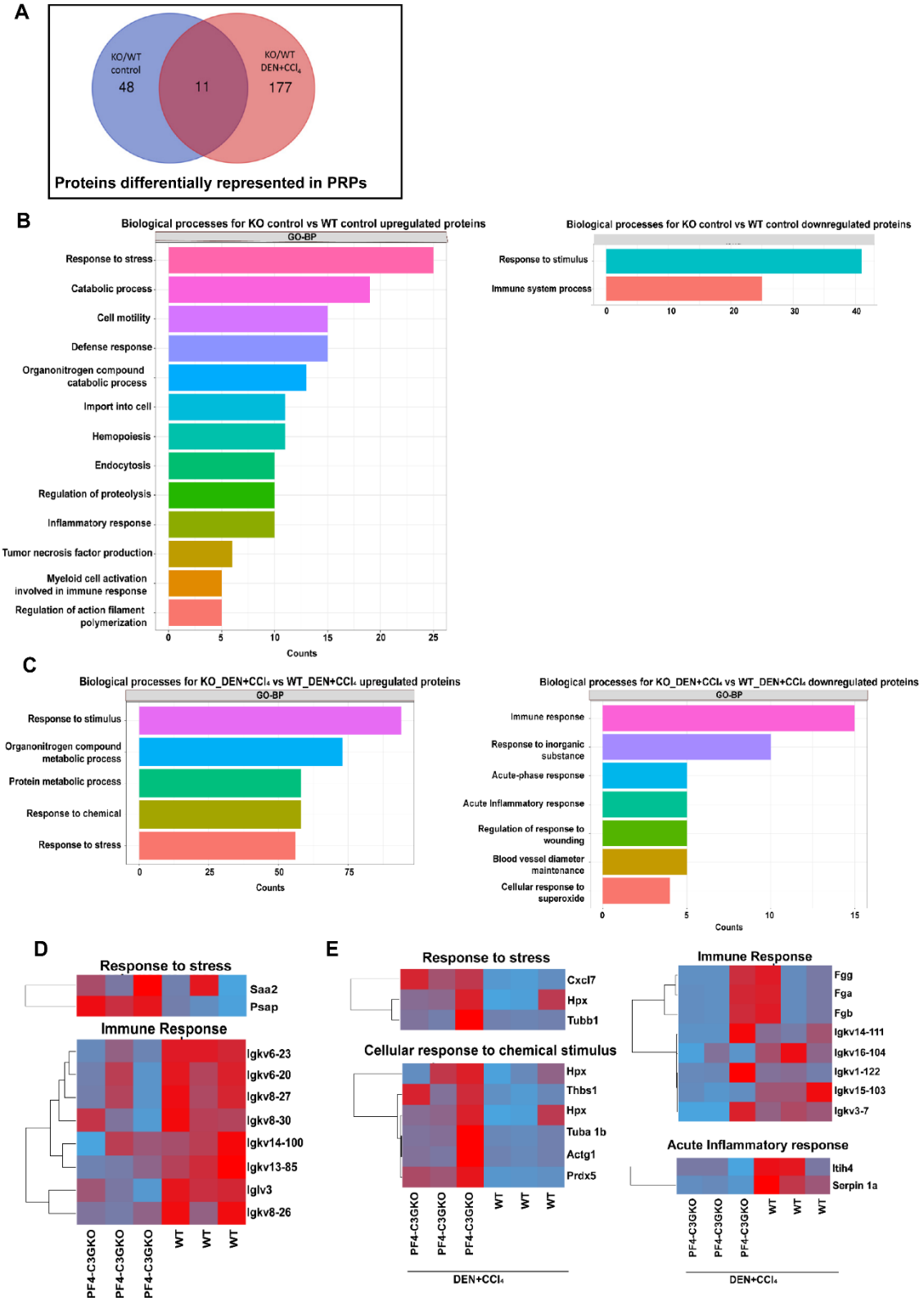

Supplementary figure 10-C3G deletion in platelets induces changes in platelet protein profile under basal conditions and upon chemically-induced HCC associated with fibrosis. Platelet rich plasma (PRP) of mice lacking C3G in megakaryocytes and platelets (PF4-C3GKO) and their corresponding wt counterparts treated with DEN+CCl_4 or vehicle (control) for 14 weeks was used for a wide proteomic analysis. A) The scheme represents the number of proteins differentially present in PRPs

from PF4-C3GKO compared with wt mice treated with DEN+CCl_4 or vehicle for 14 weeks as indicated. Bar charts showing upregulation or downregulation of proteins involved in the indicated biological processes in PF4-C3GKO vs wt PRPs found in GO-BP analysis in untreated (B) and DEN+CCl_4 treated (C) mice. (D, E) Heatmap analysis showing some of the proteins upregulated (red) or downregulated (blue) in PF4-C3GKO vs wt PRPs untreated (D) and DEN+CCl_4 treated (E) mice.

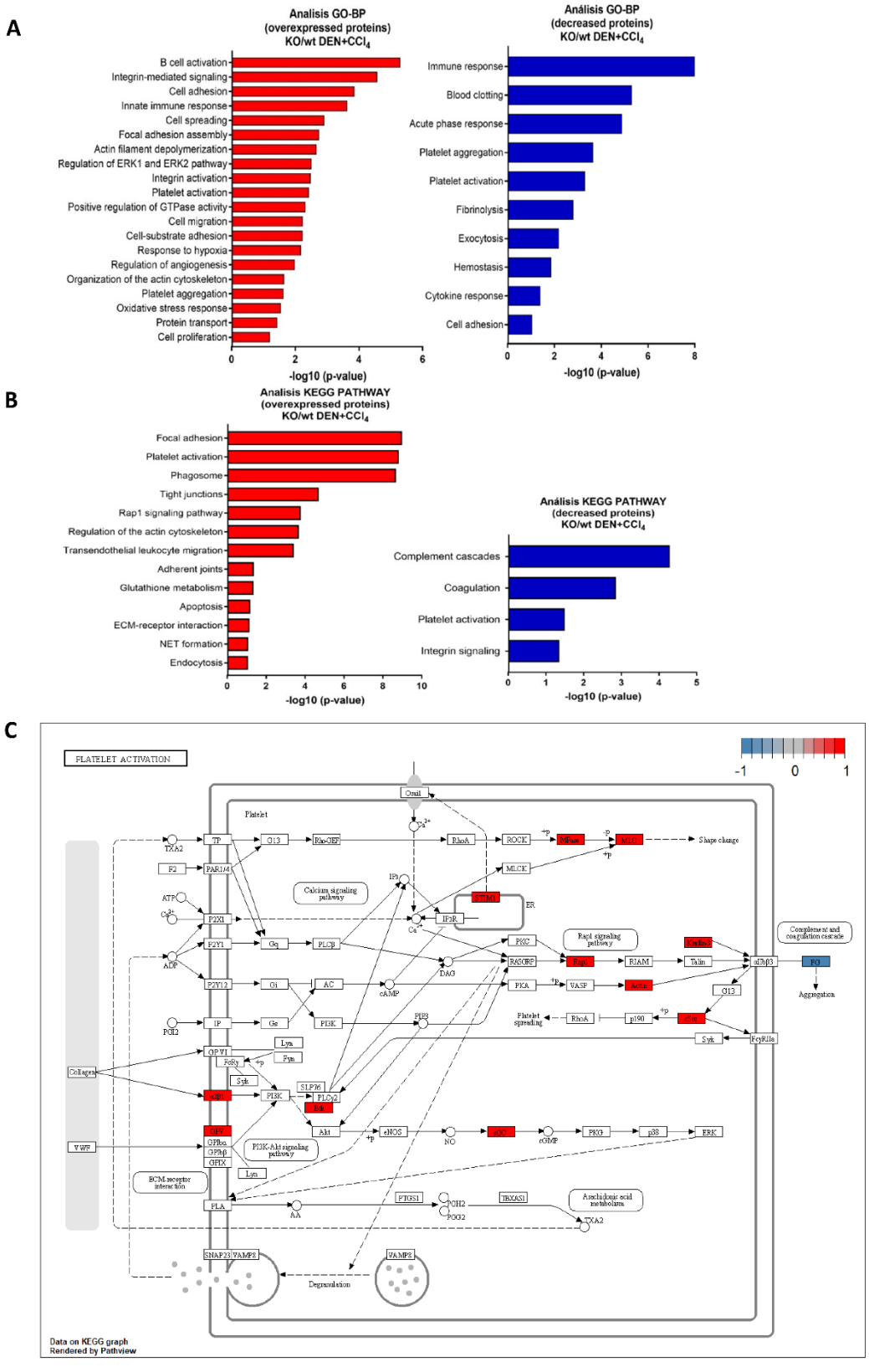

Supplementary figure 11-C3G deletion in platelets induces changes in platelet proteins involved in different biological processes in chemically-induced HCC associated with fibrosis. Enrichment analysis of biological processes using data of proteins upregulated (red) or downregulated (blue) in PF4-C3GKO as compared with wt platelet rich plasma (PRPs). Bar chart showing upregulation or downregulation of

proteins involved in the indicated biological processes in PF4-C3GKO vs wt PRPs treated with DEN+CCl_4 for 14 weeks found in GO-BP (A) and KEGG (B) analyses. It is represented -log10 of p value obtained from the statistical method applied. C) Scheme showing proteins from platelet activation pathways (e.g. GPV, $\alpha 2\beta 1$ integrin, Rap1 or c-Src), that are upregulated (red) in PF4-C3GKO as compared with wt PRPs from mice treated with DEN+CCl_4 for 14 weeks derived from KEGG analyses.

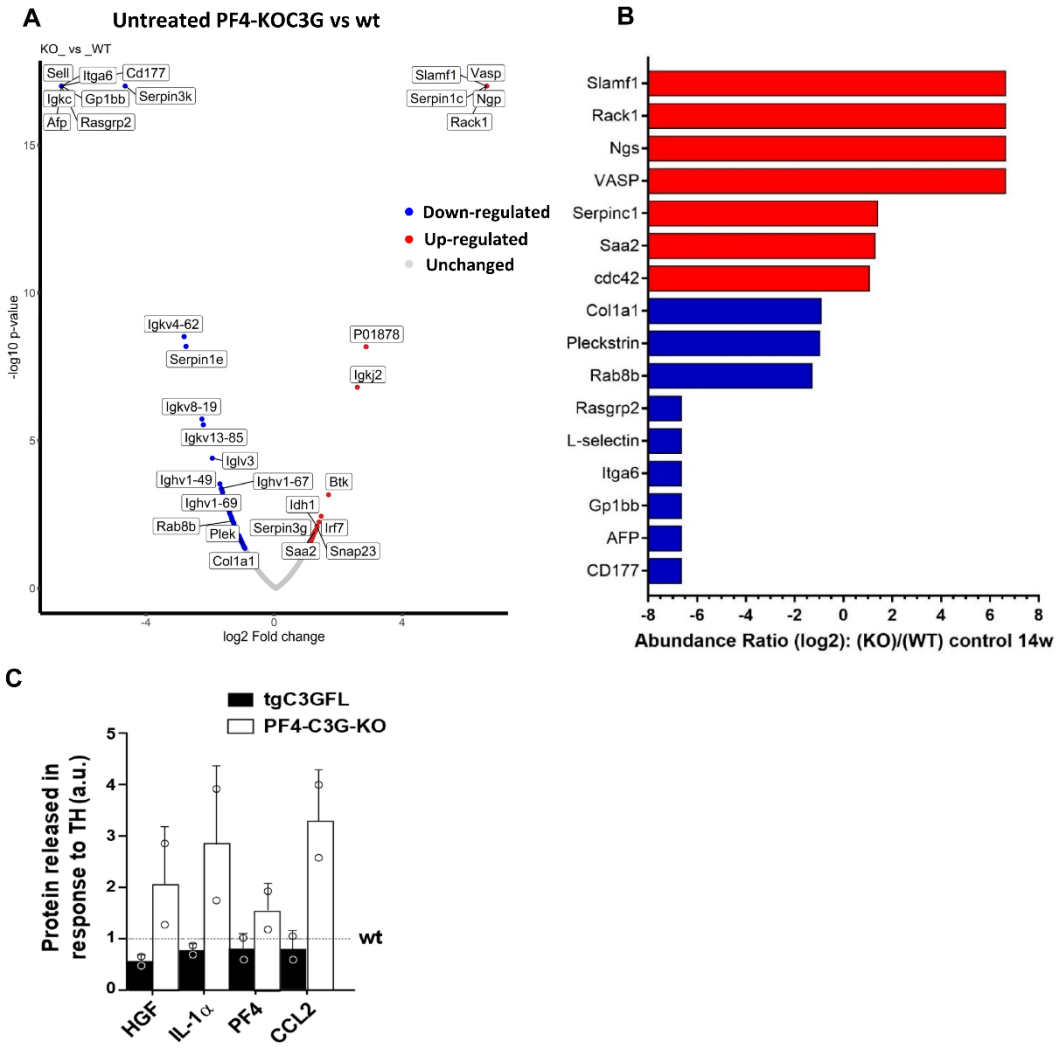

Supplementary figure 12-Deletion of C3G in platelets induces changes in the proteins present in platelet rich plasma upon chemically induced liver cancer associated with fibrosis. Wide proteomic analysis of platelet rich plasma (PRP) comparing untreated mice lacking C3G (PF4-C3GKO) in megakaryocytes and platelets with their corresponding wt counterparts. A) Volcano plot and B) bar chart show proteins upregulated (in red), downregulated (in blue) or unaffected (in grey) in PF4-C3GKO vs wt PRPs. C) Histogram represents the quantification of HGF, IL-1α, PF4 and CCL2 levels in thrombin-induced secretome from PF4-C3GKO platelets and their controls, using the Proteome Profiler Mouse Angiogenesis Array Kit (R&D Systems), (n=2, each per duplicated).

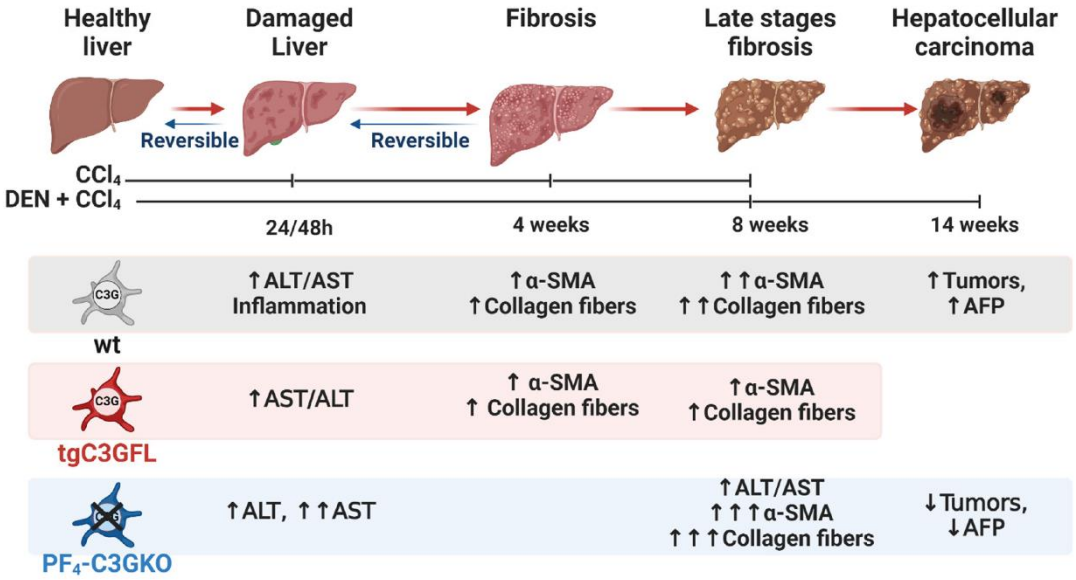

Supplementary figure 13-Scheme showing the predictive liver damage induced by CCl_4 and DEN+CCl_4 over time. Regulation by platelet C3G. Changes in the activity of ALT (alanine amino transferase) and AST (aspartate amino transferase), inflammation, collagen accumulation, α-SMA (α-Smooth muscle actin) levels, number and size of tumors and the expression of α-Fetoprotein (AFP) associated with different levels of liver damage and HCC (hepatocellular carcinoma) development are shown, as well as the impact of either overexpression of full length C3G (C3GFL) or its deletion in platelets (C3GKO). Short-term treatment with CCl_4 induces reversible damage (acute), which can progress to fibrosis upon chronic treatment with CCl_4 (for 4 to 8 weeks) or DEN+CCl_4 (for 8 to 14 weeks). Fibrosis decreases when C3G is overexpressed in platelets, while C3G deletion in platelets enhances it (at 8 weeks). Tumors become visible after treatment with DEN+CCl_4 for 14 weeks, although their number and size as well as AFP levels are lower in livers from PF4-C3GKO mice.

Supplementary table 4-Effect of platelet C3G on changes in liver immune cell populations induced by treatment with CCl_4, DEN and DEN+CCl_4 for 8 weeks. Qualitative changes in liver platelets and immune cells by CCl_4, DEN and DEN+CCl_4 in tgC3GFL, tgC3GΔCat and PF4-C3GKO mice as compared to their corresponding wt counterparts in each case. Up arrows indicate an increase compared to wt, down arrows indicate a decrease, equal sign means no differences.

	Control				CCl_4 8 weeks				DEN 8 weeks		DEN+CCl_4 8 weeks	
	wt	C3GFL	C3GKO	C3GΔCat	wt	C3GFL	C3GKO	C3GΔCat	wt	C3GKO	wt	C3GKO
Platelets (CD41+)		↑↑	=	↑↑	↑↑	↑	=	=	=	=	↑	=
Macrophages (F4/80+)		↑↑	=	↑	↑↑	↓	=	=	=	=	↑	↑↑
CD11b+			=		↑		=		↓	↓		↑↑↑
Ly6G+			=		↑↑↑		↑				↑	↑↑

Supplementary table 5-Effect of platelet C3G on changes in liver immune cell populations induced by treatment with CCl_4, DEN and DEN+CCl_4 for 14 weeks. Qualitative changes in liver platelets and immune cells by CCl_4, DEN and DEN+CCl_4 in tgC3GFL, tgC3GΔCat and PF4-C3GKO mice as compared to their corresponding wt counterparts in each case. Up arrows indicate an increase compared to wt, down arrows indicate a decrease, equal sign means no differences.

	Control		CCl_4 14 weeks		DEN 14 weeks		DEN+CCl_4 8 weeks	
	wt	C3GKO	wt	C3GKO	wt	C3GKO	wt	C3GKO
Platelets (CD41+)		=	↑↑	=	=	=	↑	=
Macrophages (F4/80+)		=	=	=	↓	=	↓	↑
CD11b+		=	↑↑↑	↑↑	↓	↓	↑↑	↑
Ly6G+		=	↑↑↑	↑↑	=	=	↑↑	↑